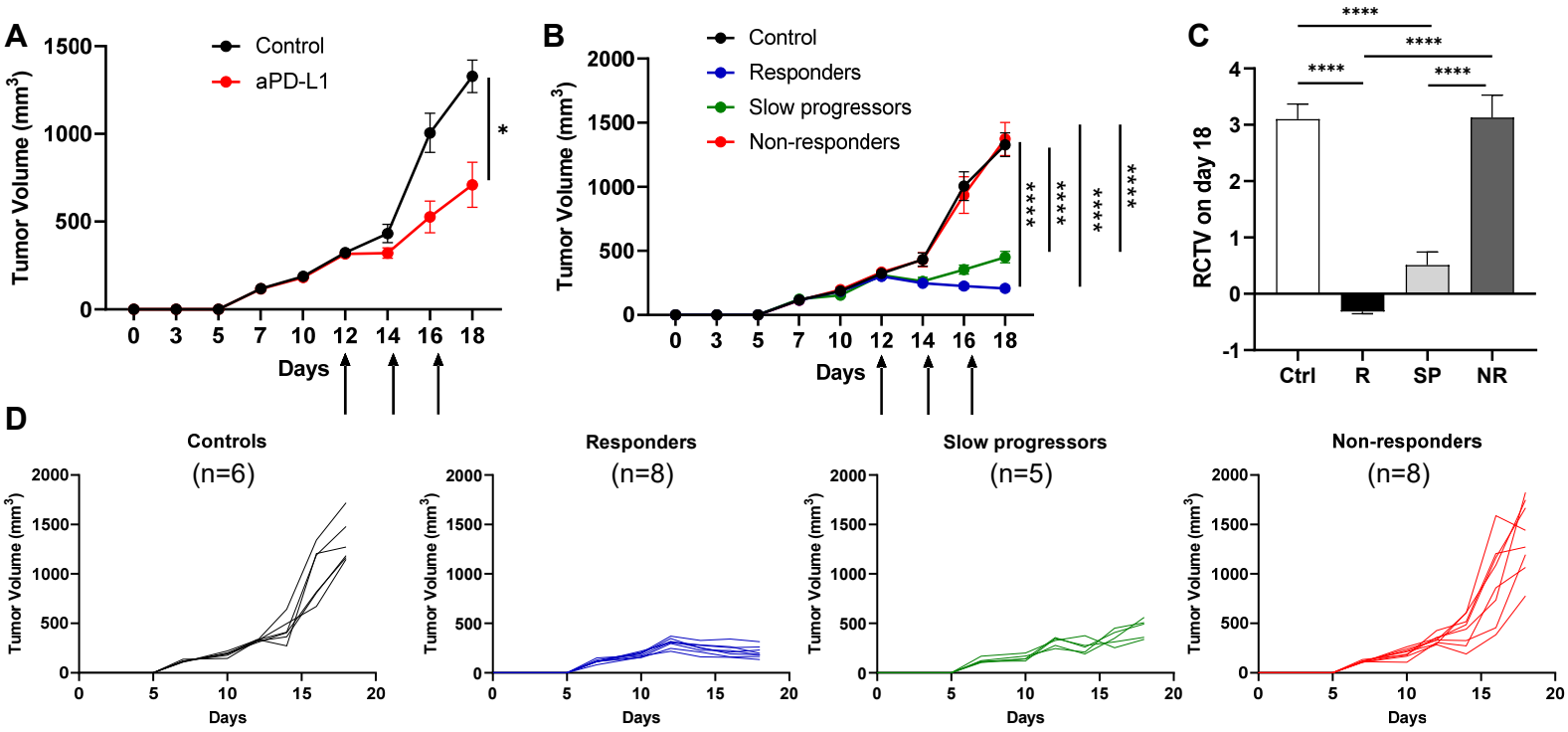

Supplemental Figure 1. Differential responses to anti-PD-L1 treatment in A223 tumor-bearing mice. A223 tumor cells (1×10^5) were injected s.c. into one flank of WT B6 mice (n=30, 90% take rate). When the tumor size reached ~300mm^3, recipients were treated with control (n=6) or anti-PD-L1 mAb (n=21) for 3 times (2-day intervals). Tumor growth was monitored for 18 days. Arrows indicate anti-PD-L1 treatment. **(A)** Overall tumor growth curves of control (n=6) and anti-PD-L1-treated (n=21) mice. **(B)** Tumor growth curves of control, responder (R), slow progressor (SP) and non-responder (NR) groups. According to relative change in tumor volume (RCTV) on day 18, anti-PD-L1 treated recipients diverged into R (n=8, RCTV<0), SP (n=5, 0<RCTV≤1.5) and NR (n=8, RCTV>1.5) **(C)** RCTV of control and different treatment groups (R, SP and NR). RCTV is calculated as the change in tumor volume (TV) from the start of treatment (day 12) to the endpoint date of the control group (day 18) divided by TV at day 12 ($TV_{day18}-TV_{day12})/TV_{day12}$. **(D)** Individual tumor growth curves of controls, R, SP, and NR groups. Data were presented as mean ± SEM. Statistical significance was calculated with unpaired t test or one-way ANOVA followed by Tukey's multiple comparisons test (*, *P*<0.05; ****, *P*<0.0001).

Supplemental Figure 1A-D

A

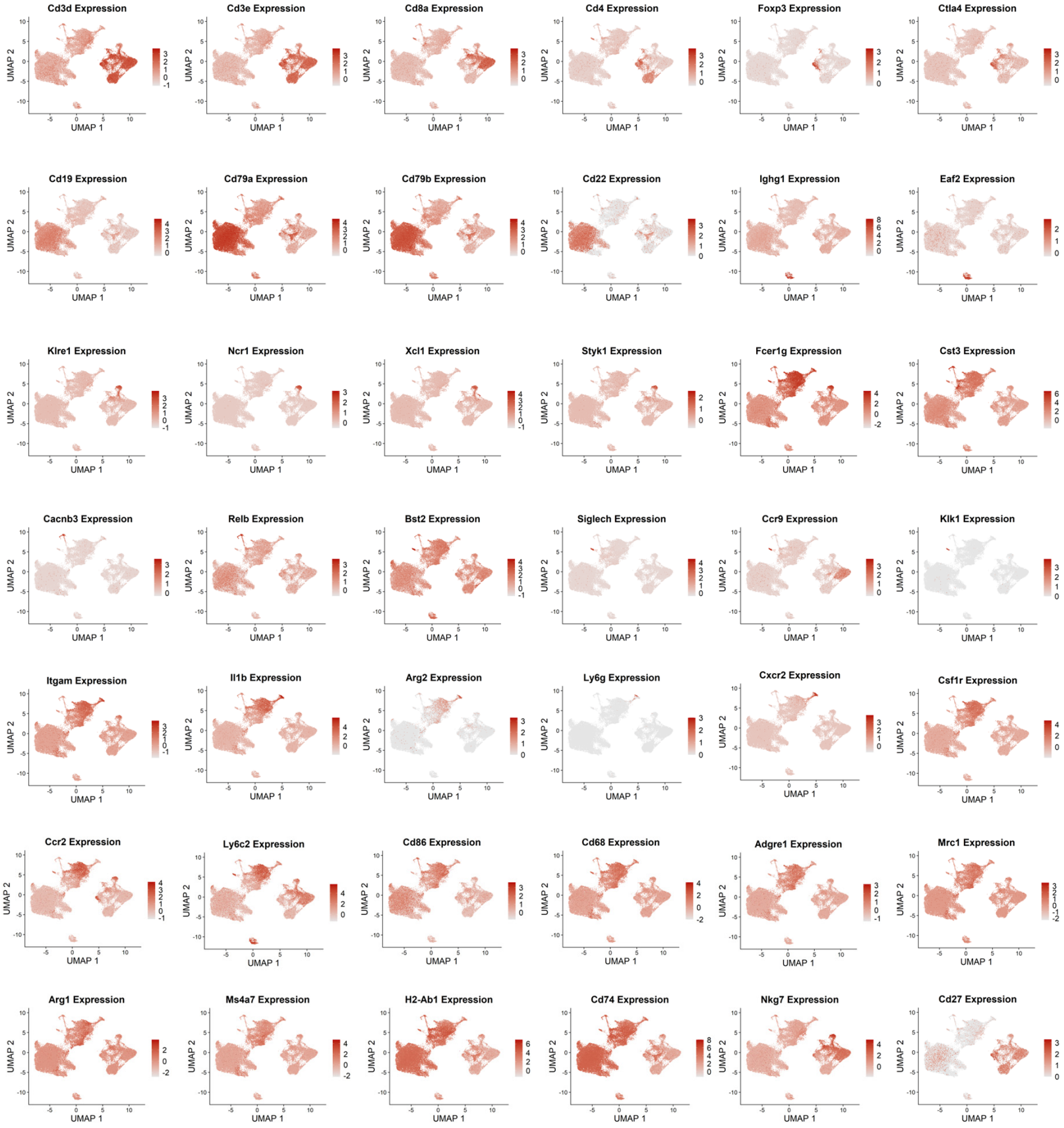

Supplementary Figure 2A

B

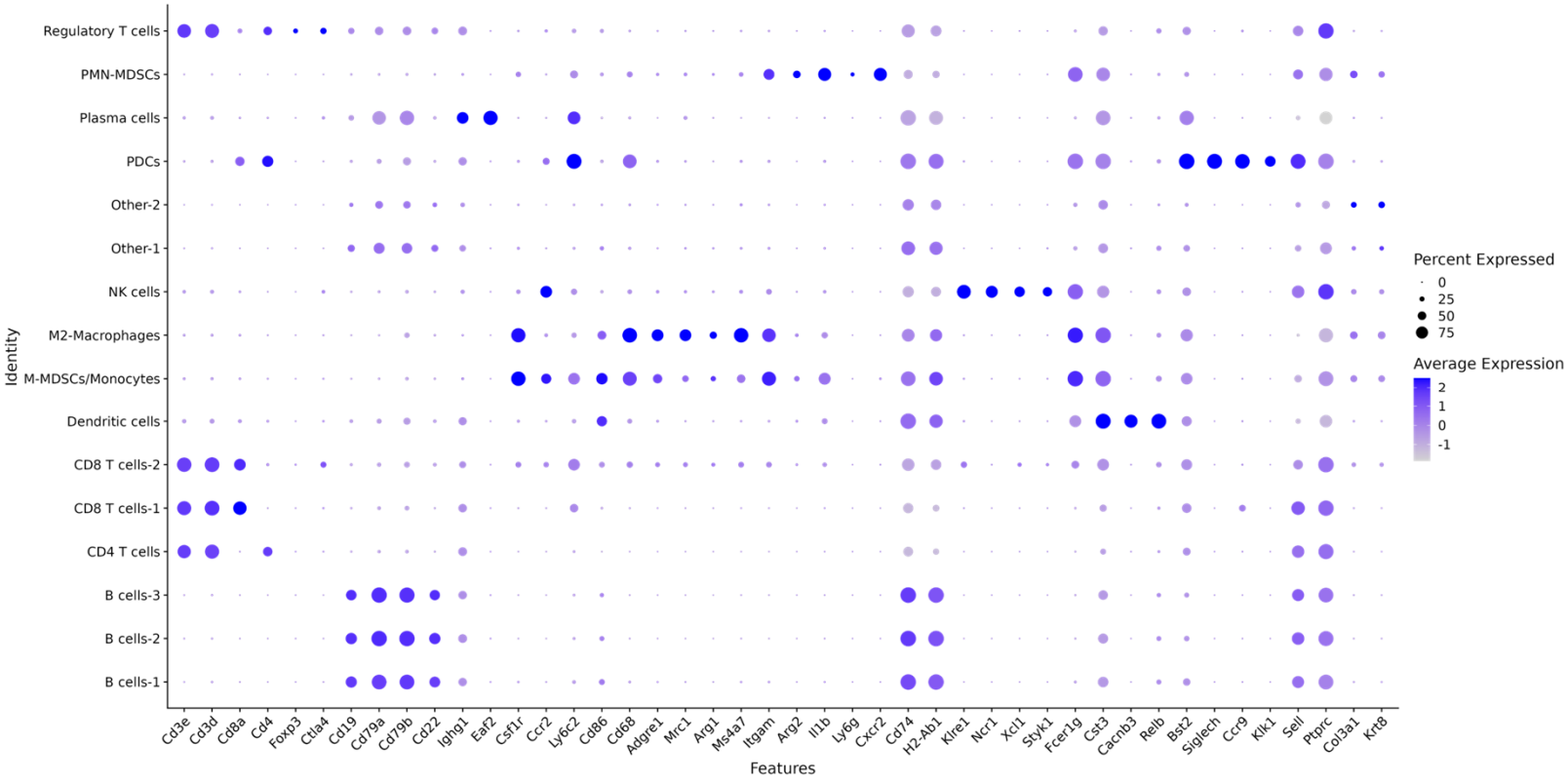

Supplemental Figure 2. Gene annotation for different cell clusters. (A) UMAP plots showing the normalized expression of 42 representative genes in different clusters (gray=little to no expression; red=high expression). **(B)** Dot plot showing the expression of representative genes for each cluster of the UMAP plot. This plot displays both the average expression level (color intensity) and the percentage of cells expressing each marker (dot size).

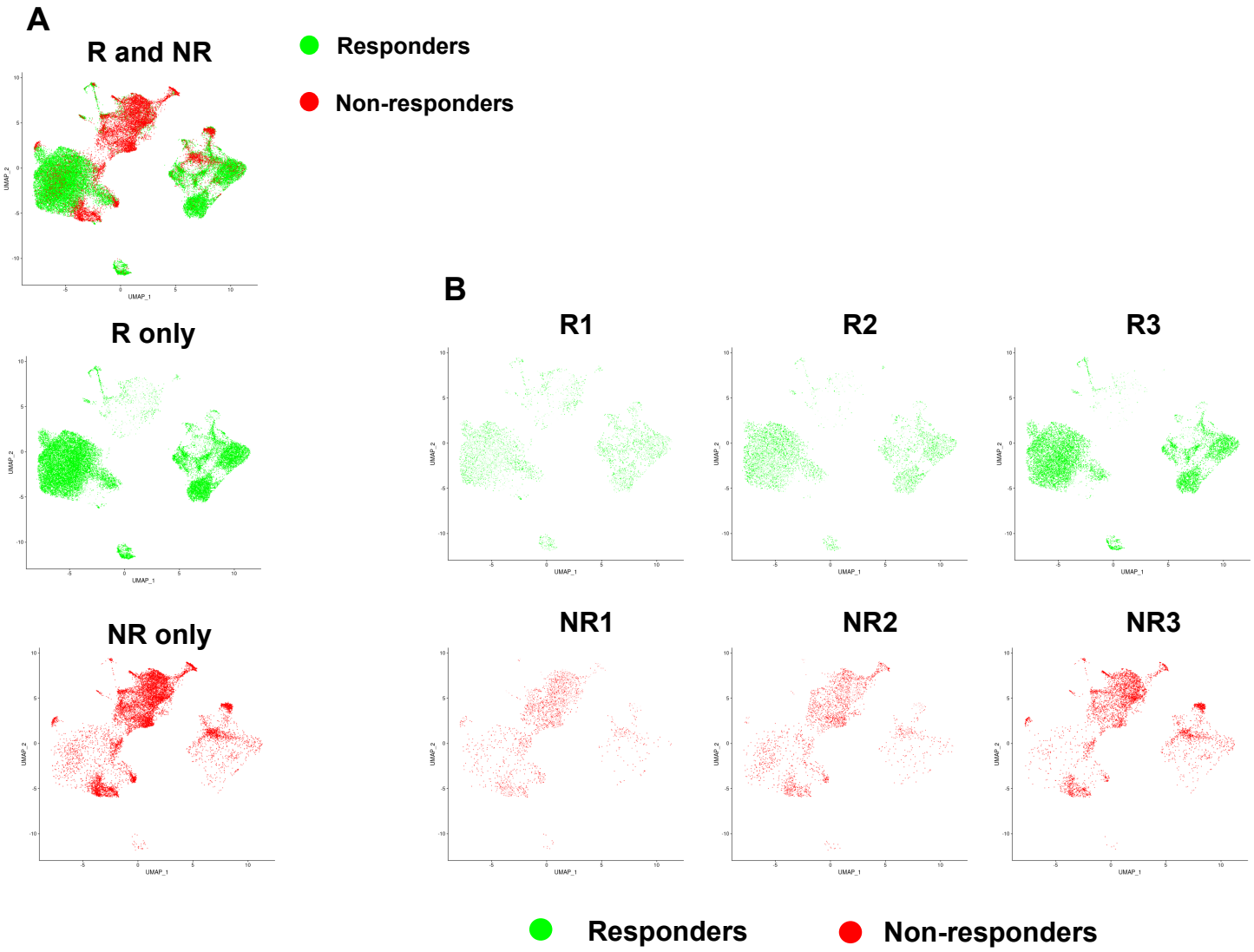

Supplemental Figure 3. Single cell RNA-seq analysis of responder (R) versus non-responder (NR) TILs from A223 tumors. CD45^{+} cells were isolated from the tumors of 3 R and 3 NR mice treated with anti-PD-L1 and subjected to scRNA-seq. **(A)** UMAP plots of different samples shown as either superimposed or separately for R TILs (green) or NR TILs (red). **(B)** UMAP plots of individual samples (R1, R2, R3, NR1, NR2, and NR3) shown separately.

A

Characteristic	HR	95% CI	p-value
AGE	1.02	1.01, 1.03	0.004
SEX			0.11
Female	—	—	
Male	0.77	0.57, 1.05	
RACE			0.14
American Indian or Alaska Native	—	—	
Asian	1.87	0.21, 17.0	
Black or African American	2.66	0.36, 19.9	
White	1.53	0.21, 11.0	
LGALS1	1.17	1.04, 1.32	0.010

Abbreviations: CI = Confidence Interval, HR = Hazard Ratio

B

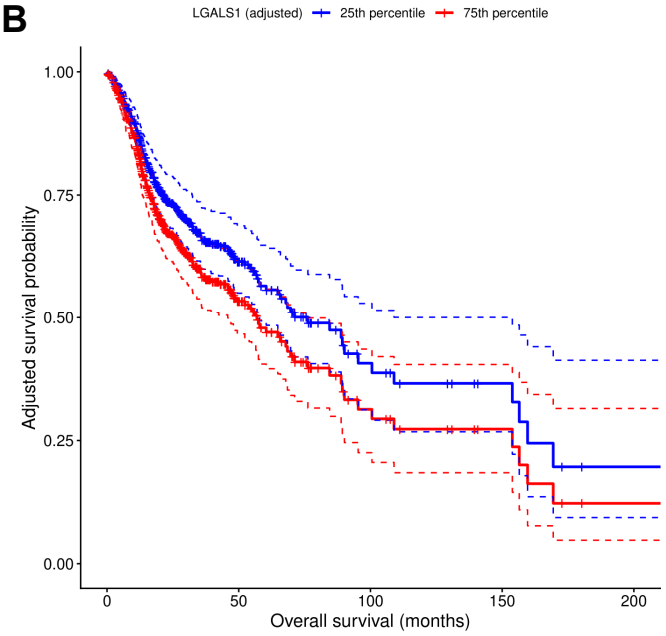

C

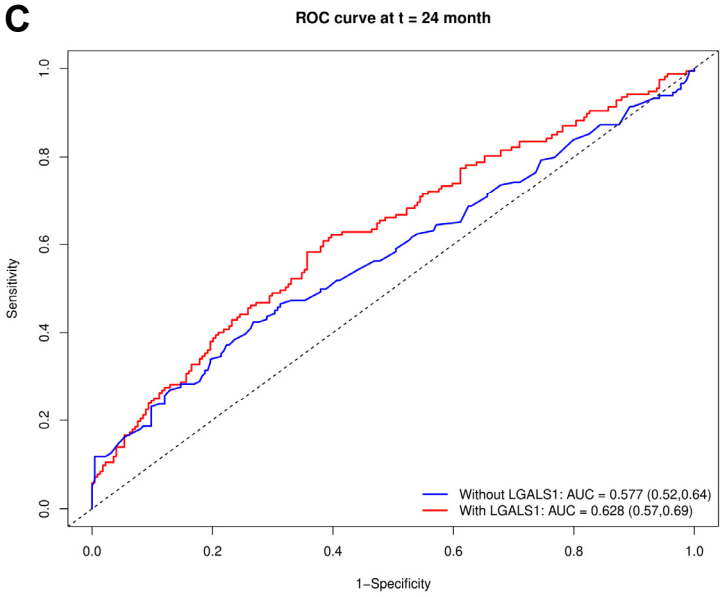

method AUC	t = 24 months	t = 36 months
with LGALS1	0.628 (0.57, 0.69)	0.620 (0.56, 0.68)
without LGALS1	0.577 (0.52, 0.64)	0.588 (0.53, 0.65)

Supplemental Figure 4. Statistical analysis of TCGA dataset. (A) Multivariable survival analyses adjusting for age, sex, and race. LGALS1 was significantly associated with OS (p = 0.010) (sample size = 500, number of events= 210). **(B)** Model-based adjusted survival curves for LGALS1 evaluated at two representative values (25th and 75th percentiles), with adjustment for age, sex, and race. For visualization, sex was fixed at male, race was fixed at White, and age was fixed at its median value. Lower LGALS1 expression correlated with a higher survival probability. **(C)** Time-dependent AUC analyses at 2 and 3 years. **Left**, ROC curve at 24 months; **Right,** AUC analyses were performed to compare the performance of the full model with that of a baseline model excluding LGALS1. Consistent improvements in AUC were observed across all evaluated time points.

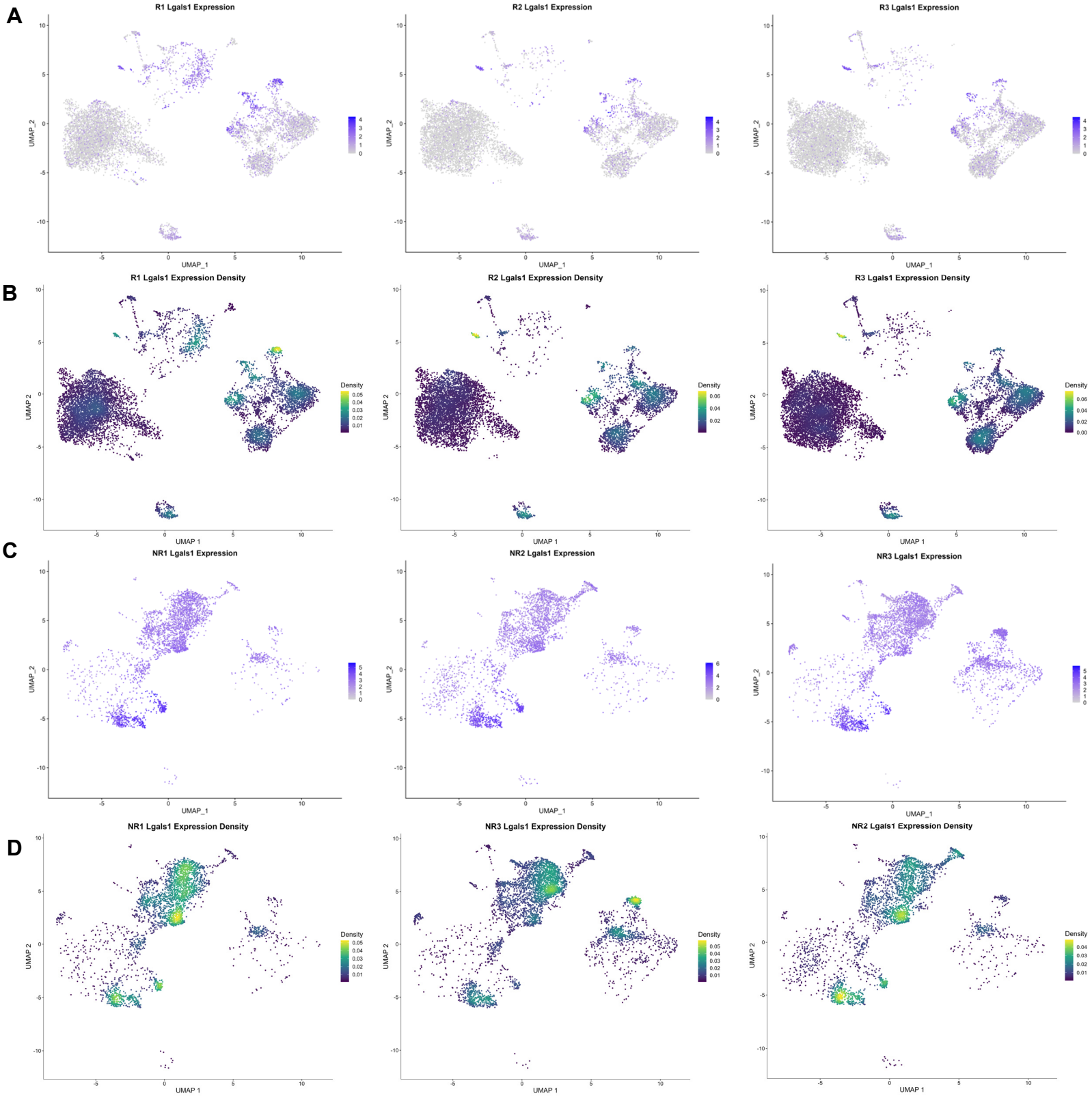

Supplemental Figure 5: LGALS1 expression in Responder (R) and Non-Responder (NR) tumor-infiltrating CD45⁺ cells. CD45⁺ cells were isolated from the tumors of 3 R and 3 NR mice treated with anti-PD-L1 and subjected to scRNA-seq. **(A, C)** UMAP of visualization of LGALS1 expression in the tumor infiltrating CD45⁺ cells from each R (R1, R2, R3) **(A)** or NR (NR1, NR2, NR3) **(C)** sample. **(B, D)** UMAP of visualization of LGALS1 expression with cellular density considering both transcript level and cell density (% of cells expressing the LGALS1 transcript) in the tumor infiltrating CD45⁺ cells from each R (R1, R2, R3) **(B)** or NR (NR1, NR2, NR3) **(D)** sample.

Supplemental Figure 5A-D

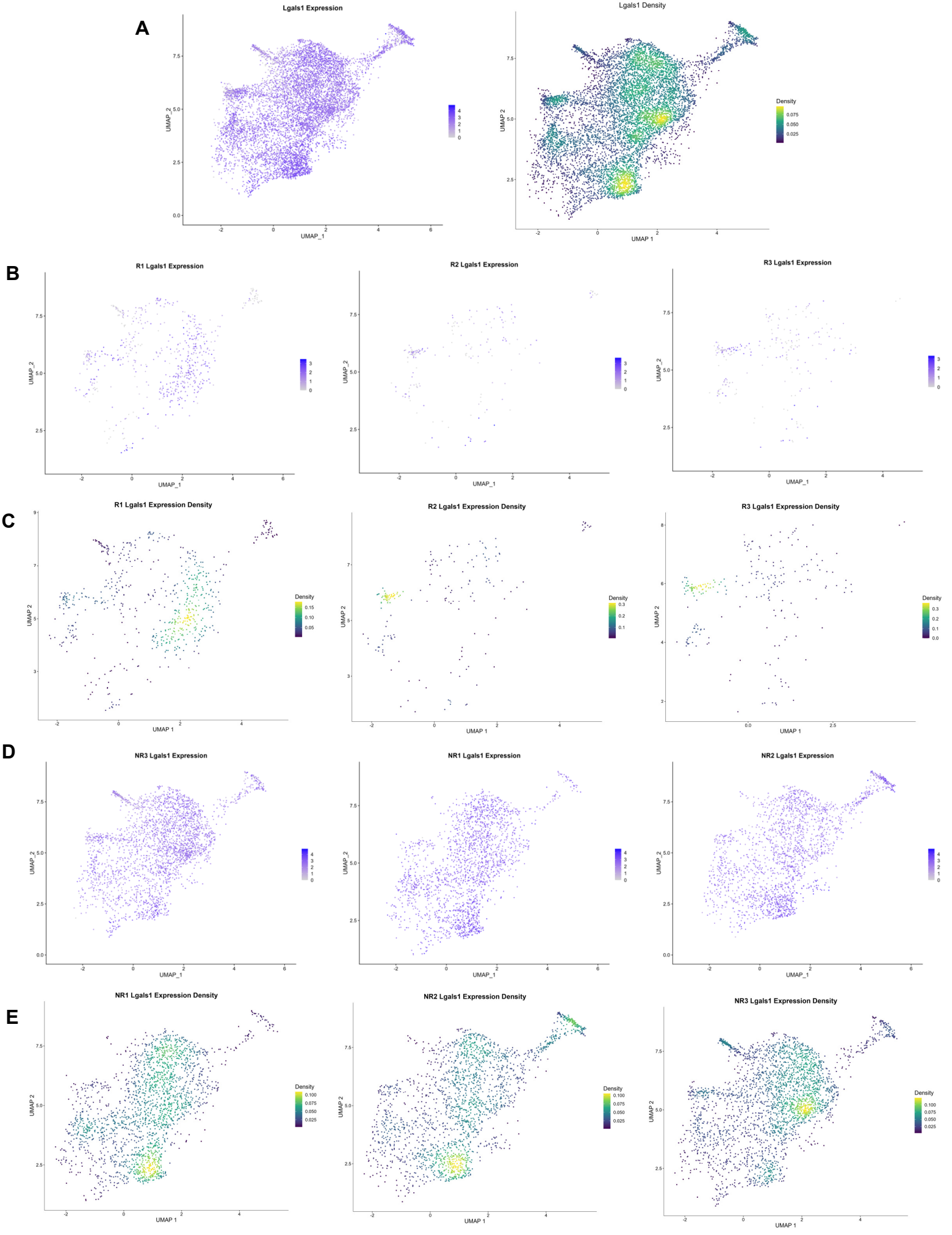

Supplemental Figure 6A-E

Supplemental Figure 6: LGALS1 expression in Responder (R) and Non-Responder (NR) tumor-infiltrating myeloid cells. $CD45^+$ cells were isolated from the tumors of 3 R and 3 NR mice treated with anti-PD-L1 and subjected to scRNA-seq. **(A)** UMAP of visualization of LGALS1 expression **(left)** and UMAP of visualization of LGALS1 expression with cellular density considering both transcript level and cell density (% of cells expressing the LGALS1 transcript) **(right)** in the tumor infiltrating myeloid cells from combined R (n=3) and NR (n=3) samples. UMAP of visualization of LGALS1 expression **(B, D)** and LGALS1 expression with cellular density **(C, E)** in myeloid cells from each R (R1, R2, R3) or NR (NR1, NR2, NR3) sample.

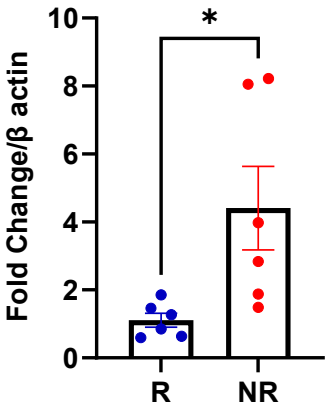

Supplemental Figure 7. Real-time PCR analysis of LGALS1 transcript in CD11b⁺ tumor-infiltrating myeloid cells from responder (R) vs. non-responder (NR). Quantification of real-time PCR data using RNA samples from R vs. NR CD11b⁺ tumor-infiltrating myeloid cells (n=3/group). Data were pooled from two independent experiments. Statistical significance was calculated with unpaired t test; *p<0.05.

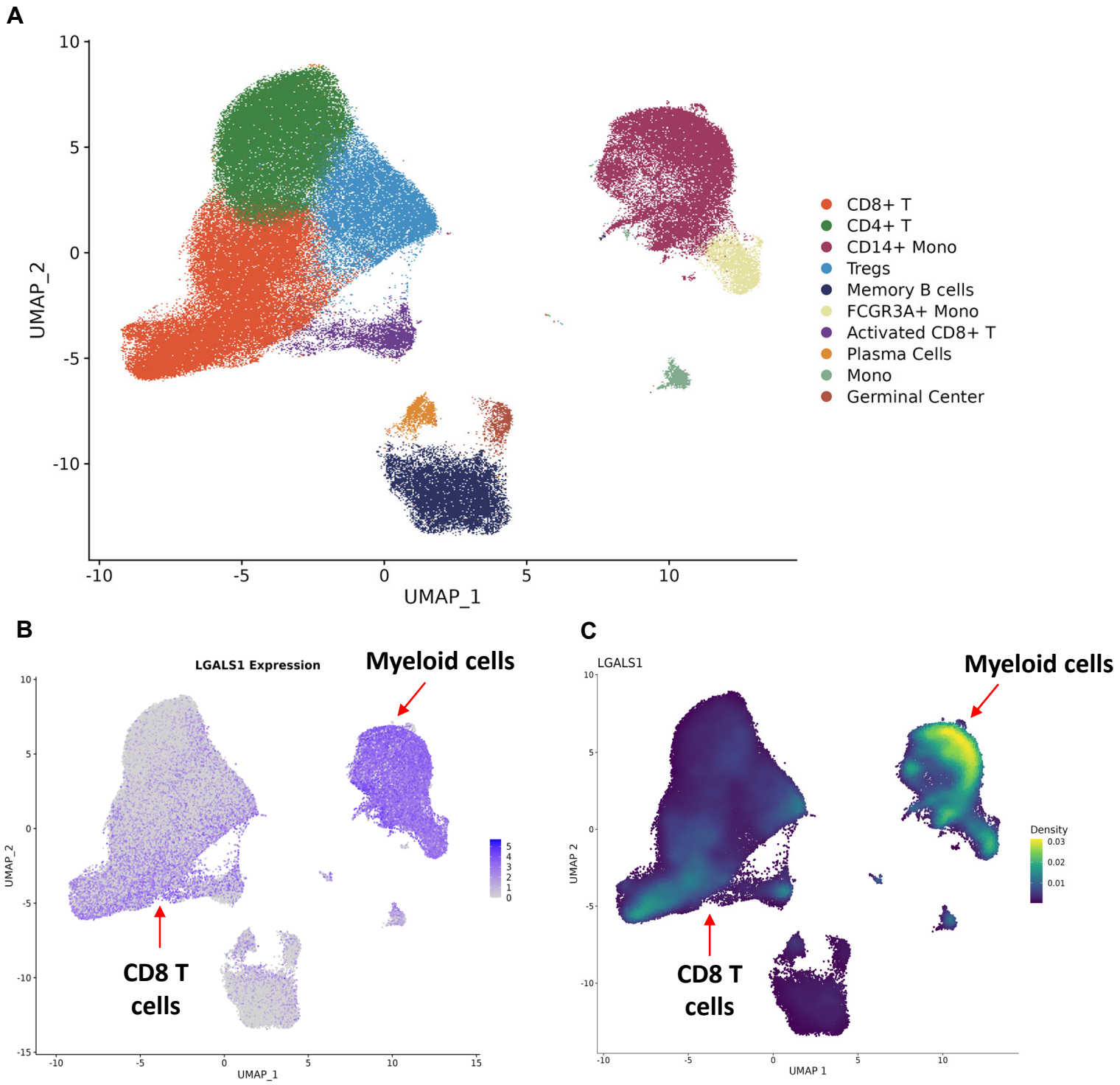

Supplemental Figure 8. LGALS1 expression in human tumor samples. (A) Cells from 58 different samples were clustered using UMAP and 10 different clusters were labeled based on gene expression. **(B, C)** LGALS1 expression in human HNSCC samples (n=58) from scRNA-seq analysis of tumor CD45 positive cells with the myeloid clusters highlighted. UMAP of visualization of LGALS1 expression **(B)**; UMAP of visualization of LGALS1 considering both transcripts level and cell density (% of cells expressing the transcript) **(C)**.

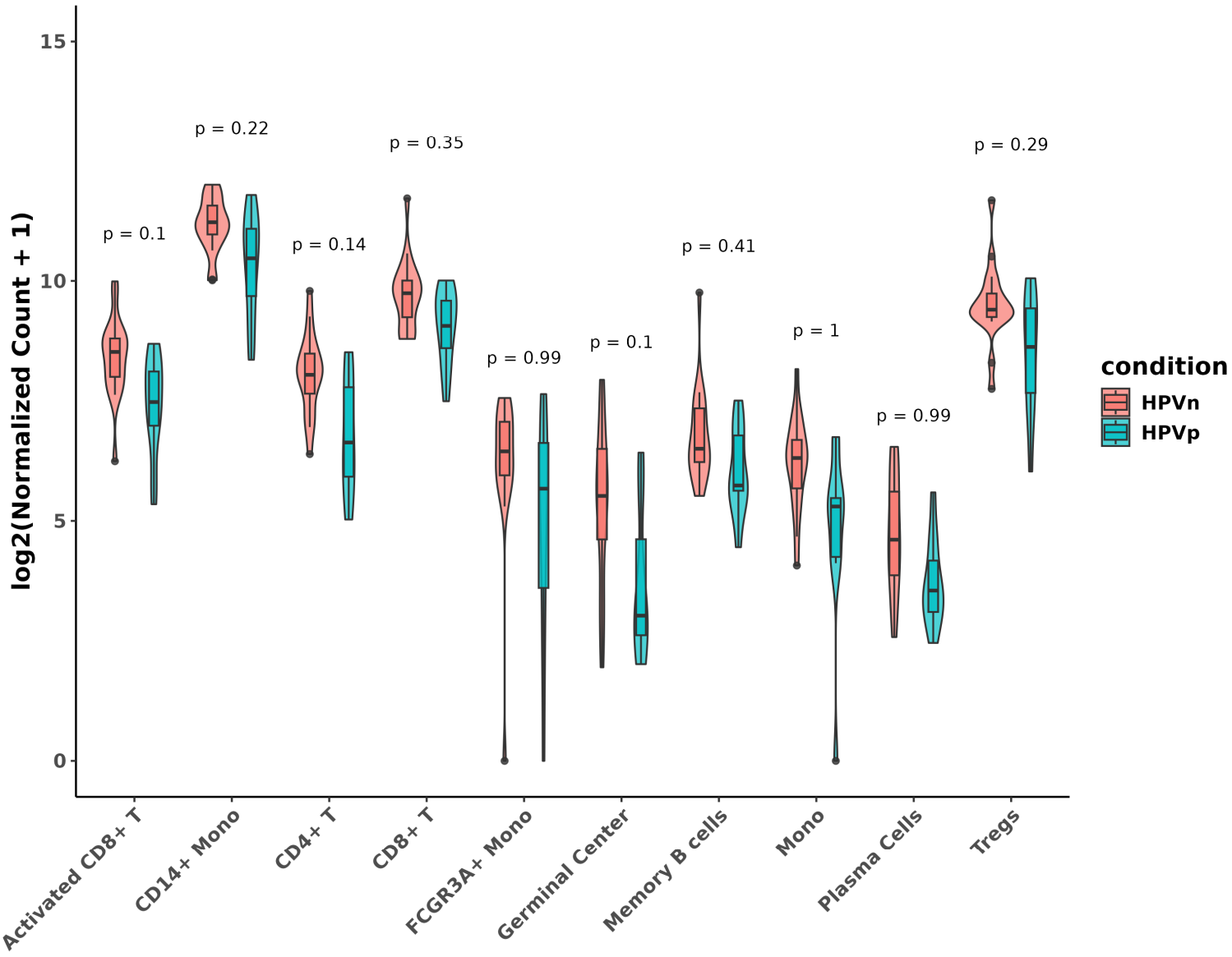

Supplemental Figure 9. No differences in LGALS1 expression between HPV⁺ and HPV⁻ TIL samples for any subset of cells compared. Single cell RNA sequencing data were aggregated into pseudobulk samples according to each cluster using the AggregateExpression function in Seurat. DESeq2 was applied separately to each cluster to perform differential expression analysis between HPV⁺ (HPVp) samples and HPV⁻ (HPVn) samples. Violin plot displays normalized counts of LGALS1 transcript with adjusted p value from DESeq2.

A

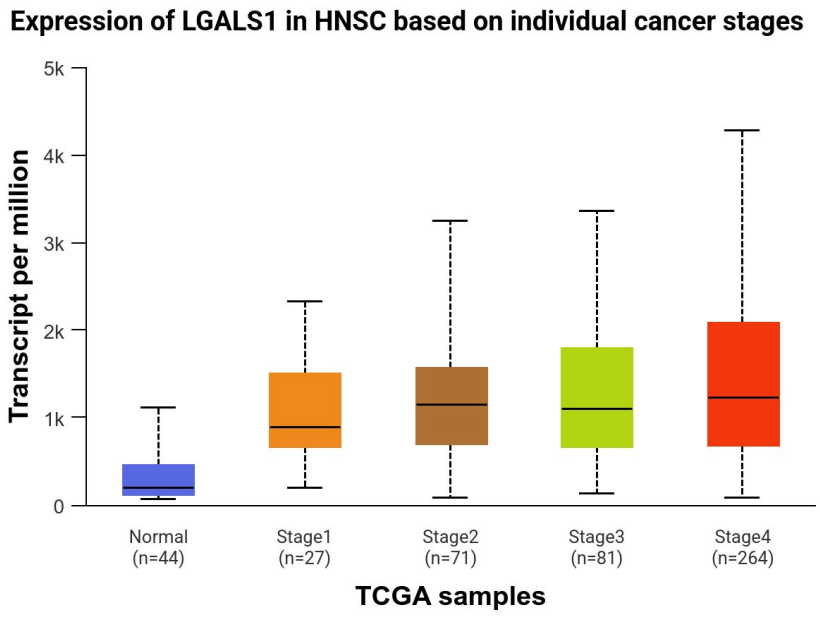

Comparison	Statistical Significance
Normal vs. Stage 1	**7.17E-04**
Normal vs. Stage 2	**1.09E-08**
Normal vs. Stage 3	**4.68E-12**
Normal vs. Stage 4	**<1E-12**
Stage 1 vs. Stage 2	8.44E-01
Stage 1 vs. Stage 3	5.36E-01
Stage 1 vs. Stage 4	5.78E-01
Stage 2 vs. Stage 3	4.92E-01
Stage 2 vs. Stage 4	2.39E-01
Stage 3 vs. Stage 4	**8.96E-03**

B

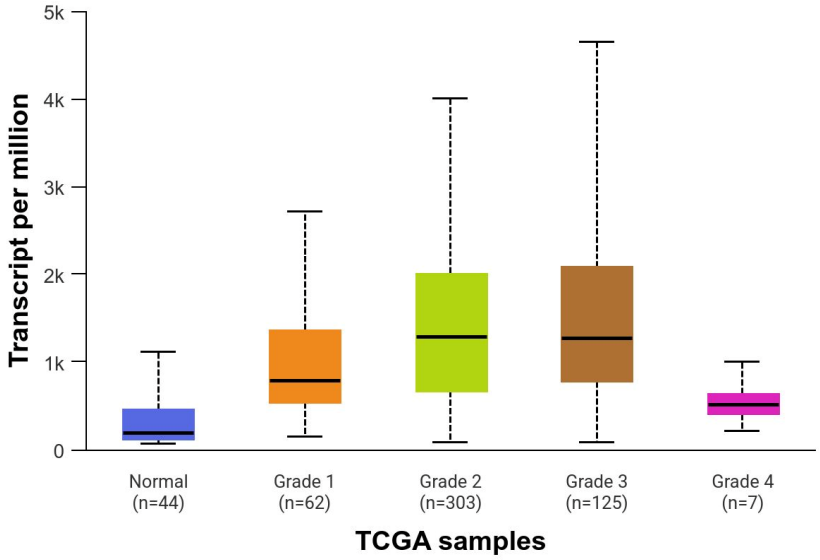

Comparison	Statistical Significance
Normal vs. Grade 1	**4.40E-08**
Normal vs. Grade 2	**1.62E-12**
Normal vs. Grade 3	**1.63E-12**
Normal vs. Grade 4	5.51E-02
Grade 1 vs. Grade 2	**1.48E-03**
Grade 1 vs. Grade 3	**9.90E-05**
Grade 1 vs. Grade 4	3.19E-01
Grade 2 vs. Grade 3	**3.63E-02**
Grade 2 vs. Grade 4	9.24E-02
Grade 3 vs. Grade 4	**6.40E-03**

Subtype descriptions

Grade 1	Well differentiated (low grade)
Grade 2	Moderately differentiated (intermediate grade)
Grade 3	Poorly differentiated (high grade)
Grade 4	Undifferentiated (high grade)

Supplemental Figure 10: LGALS1 expression in HNSC human samples. Comparison of LGALS1 expression in different subgroups of HNSC based on tumor stage (stage 1-4) **(A)** and tumor grade (grade 1-4) **(B)** in the UALCAN database. Statistical comparison is shown for each pair.

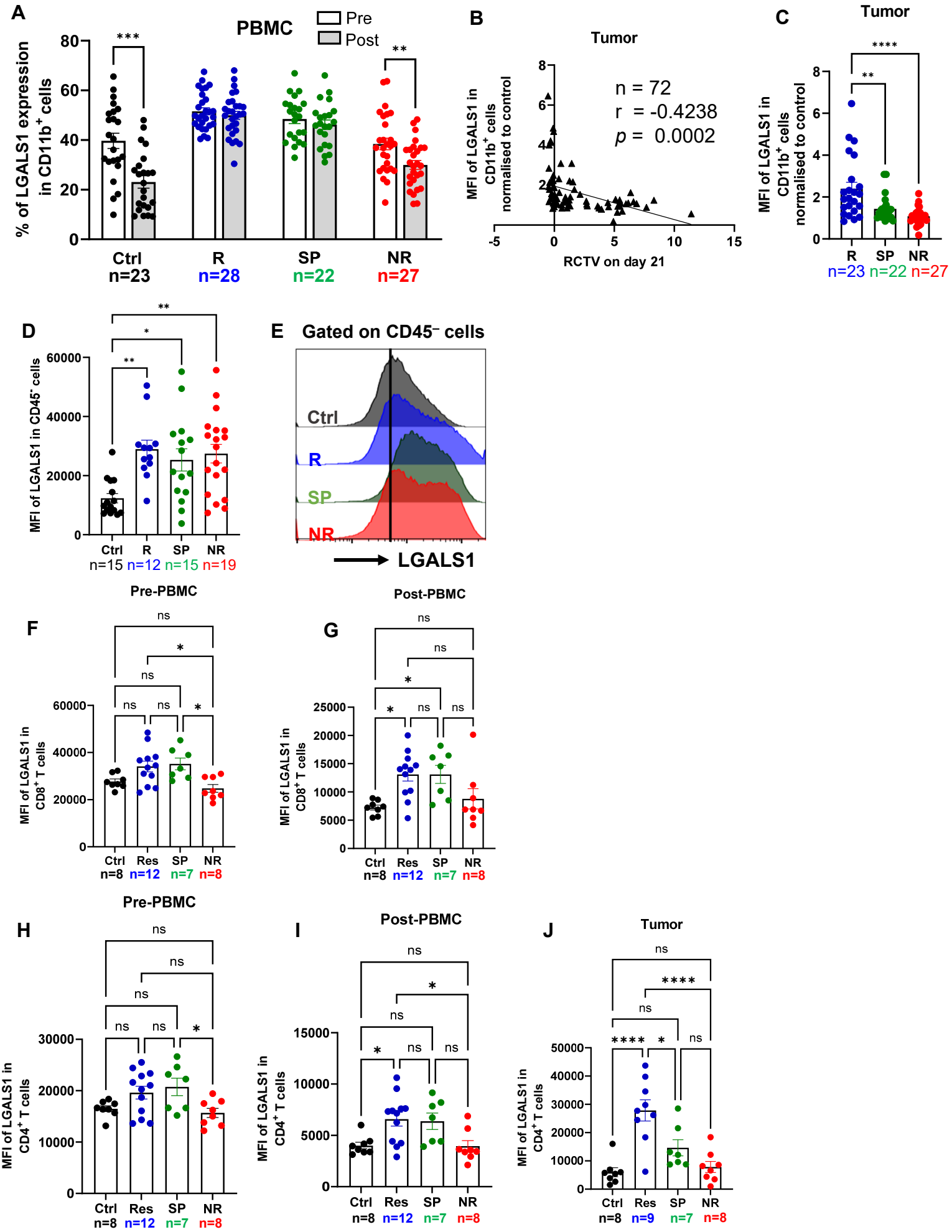

Supplemental Figure 11A-J

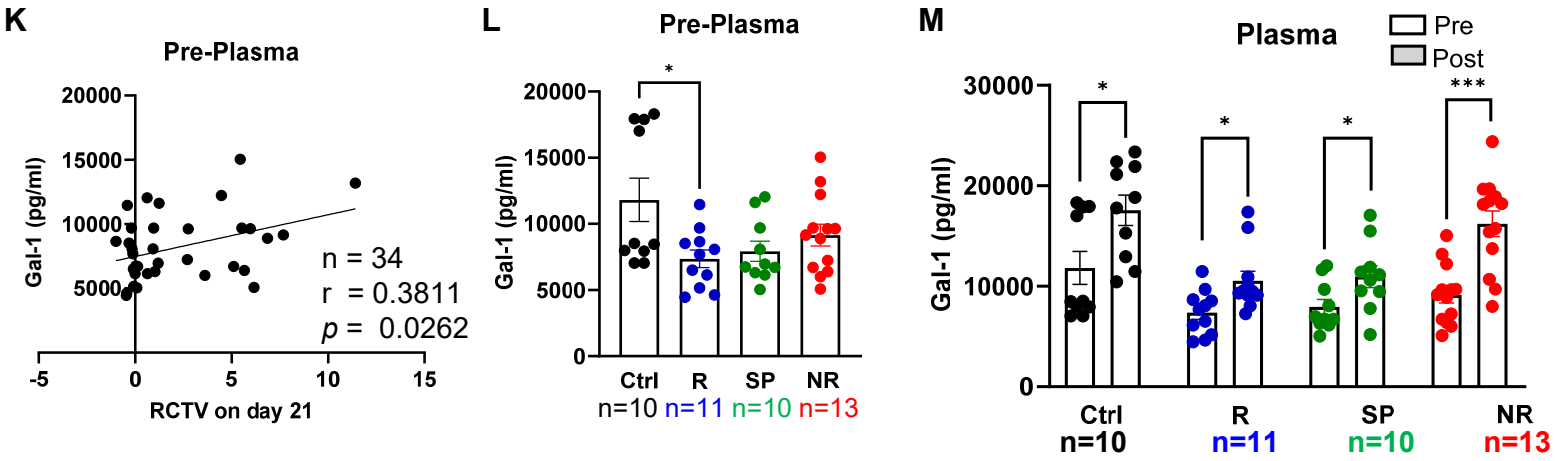

Supplemental Figure 11. Correlation of LGALS1 level with the outcome of immunotherapy treatment. A223 tumors were injected into WT B6 mice. Tumor-bearing mice were treated, and samples were collected as described in Figure 2. **(A)** Variation of intracellular levels of LGALS1 in CD11b$^+$ cells from pre- or post-PBMC samples of control and different treatment groups (R, SP and NR). **(B)** RCTV values of anti-PD-L1 treated recipients were plotted against mean fluorescence intensity (MFI) of intracellular LGALS1 in CD11b$^+$ cells from tumors normalized to the control samples and Pearson correlation coefficient was calculated. **(C)** Quantification of the MFI of intracellular LGALS1 in CD11b$^+$ cells from tumors normalized to the control samples in different treatment groups (R, SP and NR). **(D, E)** LGALS1 level in tumor cells. Quantification **(D)** and representative flow plots **(E)** showing the MFI of intracellular LGALS1 in CD45$^-$ cells from tumor samples of control and different treatment groups (R, SP and NR). **(F, G)** LGALS1 level in CD8 T cells. Quantification of the MFI of intracellular LGALS1 in CD8 T cells from Pre-PBMC **(F)** or Post-PBMC **(G)** samples of control and different treatment groups (R, SP and NR). **(H-J)** LGALS1 level in CD4 T cells. Quantification of the MFI of intracellular LGALS1 in CD4 T cells from Pre-PBMC **(H)**, Post-PBMC **(I)**, or tumor **(J)** samples of control and different treatment groups (R, SP and NR). **(K)** LGALS1 (Galectin-1, Gal-1) level in mouse pre-treatment plasma (pre-Plasma) samples was assessed by ELISA. RCTV values of anti-PD-L1 treated recipients were plotted against pre-Plasma levels of LGALS1 and Pearson correlation coefficient was calculated. **(L)** Quantification of pre-Plasma levels of LGALS1 in control and different treatment groups (R, SP and NR). **(M)** Quantification of pre- and post-Plasma levels of LGALS1 in control and different treatment groups (R, SP and NR). Data were presented as mean ± SEM. Statistical significance was calculated with one-way ANOVA followed by Tukey's multiple comparisons test (*, P<0.05; **, P<0.01; ***, P<0.001, ****, P<0.0001).

A

Characteristic	HR	95% CI	p-value
AGE	1.01	0.97, 1.05	0.7
SEX			>0.9
FEMALE	—	—	
MALE	0.96	0.37, 2.46	
LGALS1	1.07	1.01, 1.13	0.031

Abbreviations: CI = Confidence Interval, HR = Hazard Ratio

B

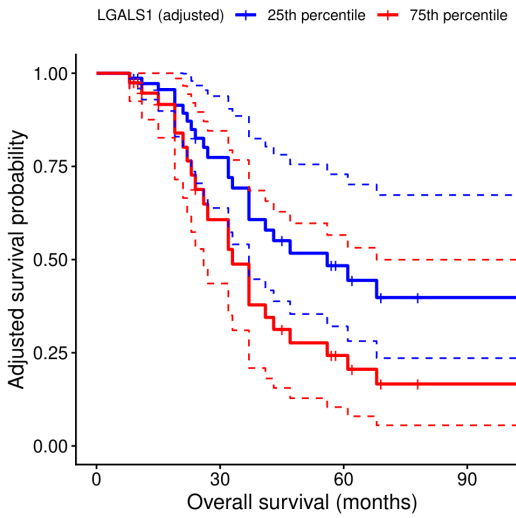

C

method	AUC t = 24 months	AUC t = 36 months
with LGALS1	0.742 (0.51, 0.98)	0.735 (0.54, 0.92)
without LGALS1	0.629 (0.36, 0.90)	0.517 (0.31, 0.72)

Supplemental Figure 12. Statistical analysis of serum patient cohort. (A) Multivariable survival analyses adjusting for age and sex. LGALS1 was significantly associated with OS ($p = 0.031$) (sample size = 41, number of events= 25). **(B)** Model-based adjusted survival curves for LGALS1 evaluated at two representative values (25th and 75th percentiles), with adjustment for age and sex. For visualization, sex was fixed at male, and age was fixed at its median value. Lower LGALS1 expression correlated with a higher survival probability. **(C)** Time-dependent AUC analyses at 2 and 3 years were performed to compare the performance of the full model with that of a baseline model excluding LGALS1. Consistent improvements in AUC were observed across both time points.

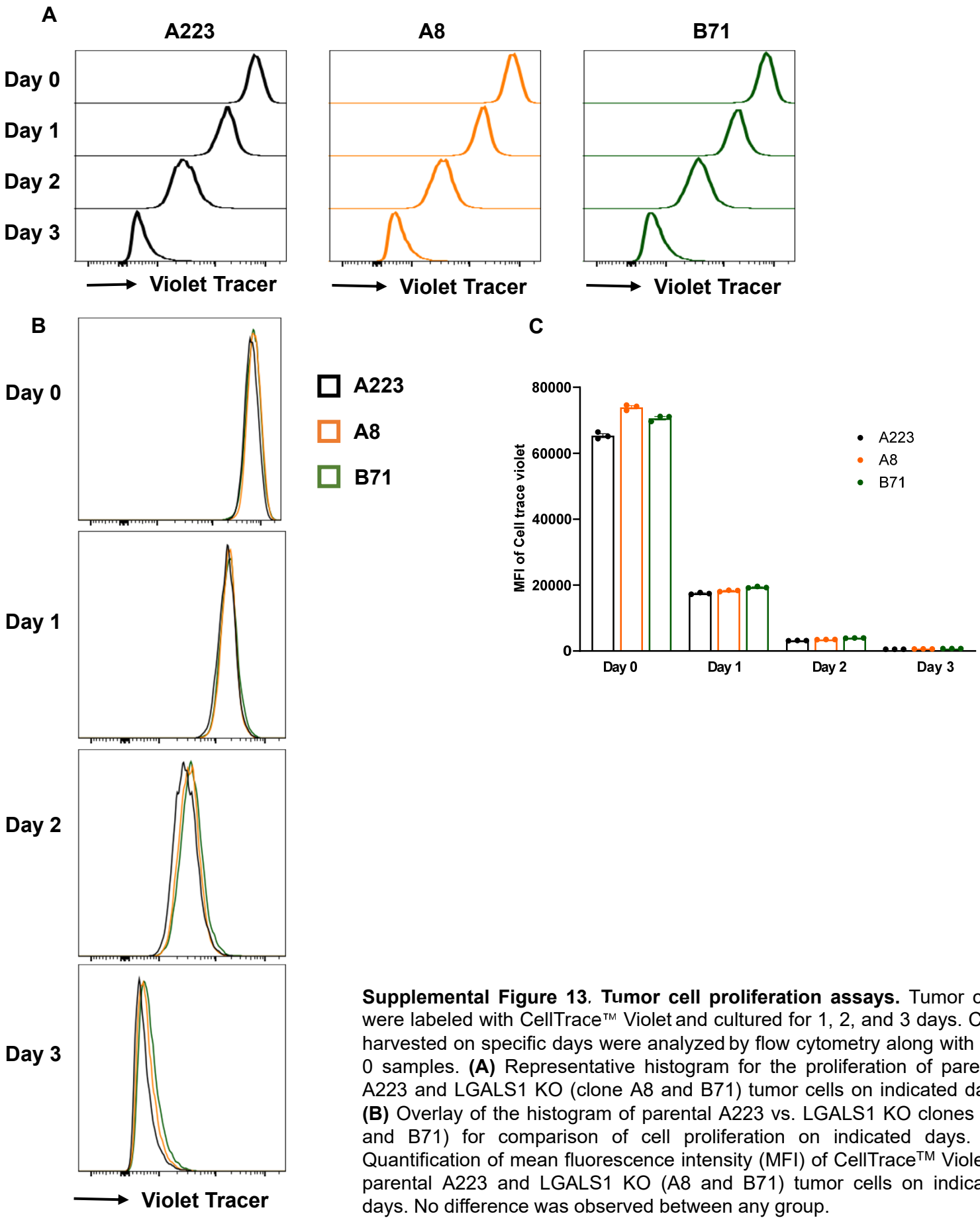

Supplemental Figure 13. Tumor cell proliferation assays. Tumor cells were labeled with CellTrace™ Violet and cultured for 1, 2, and 3 days. Cells harvested on specific days were analyzed by flow cytometry along with day 0 samples. **(A)** Representative histogram for the proliferation of parental A223 and LGALS1 KO (clone A8 and B71) tumor cells on indicated days. **(B)** Overlay of the histogram of parental A223 vs. LGALS1 KO clones (A8 and B71) for comparison of cell proliferation on indicated days. **(C)** Quantification of mean fluorescence intensity (MFI) of CellTrace™ Violet in parental A223 and LGALS1 KO (A8 and B71) tumor cells on indicated days. No difference was observed between any group.

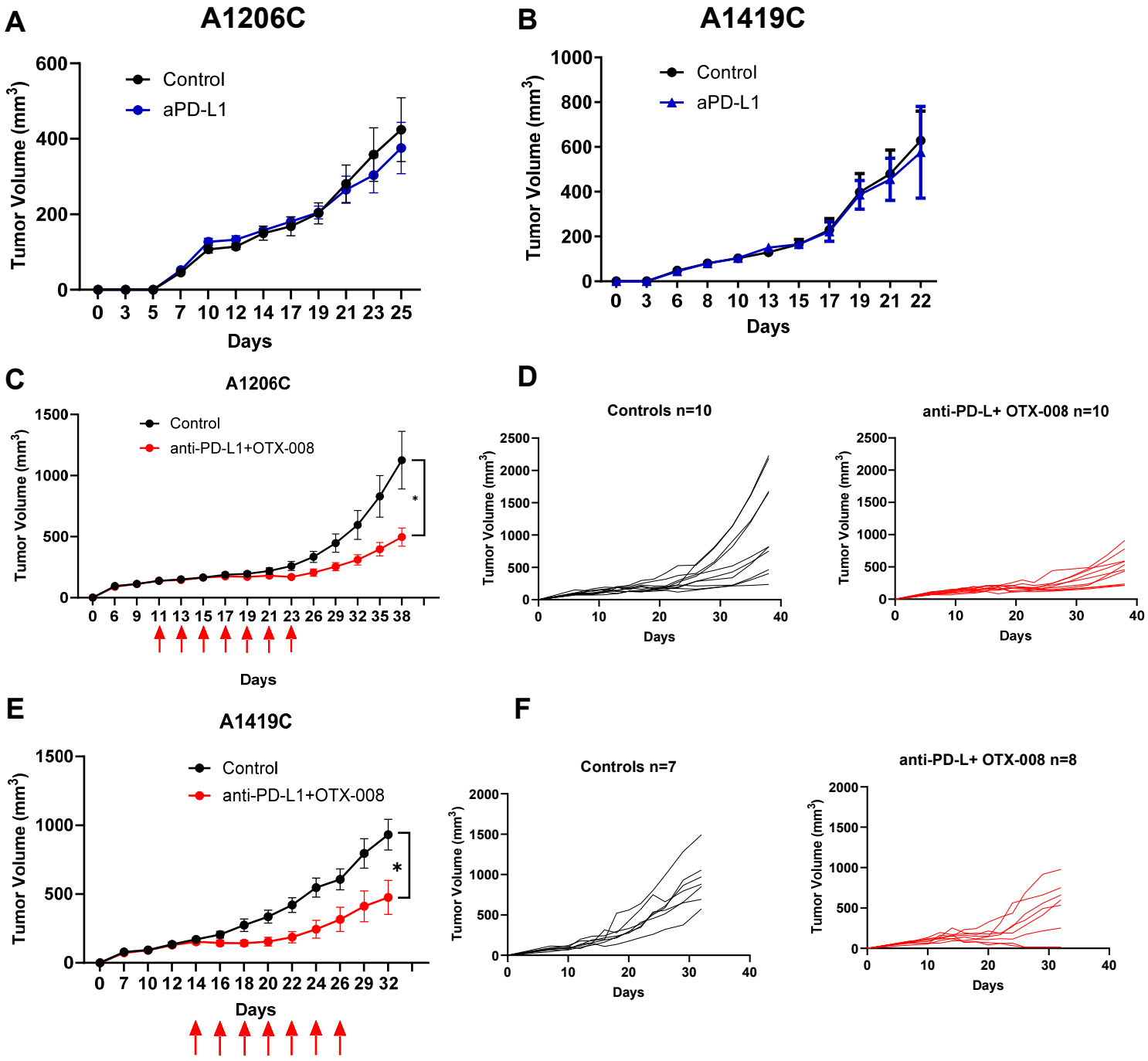

Supplemental Figure 14. OTX-008 treatment sensitizes anti-PD-L1 resistant HNSCC to combo treatment. (A, B) 4-NQO-induced SCCs (A1206C and A1419C) failed to respond to anti-PD-L1. 1×10^6 A1206C or A1419C tumor cells were injected into WT B6 recipients. When tumor size reached ~200mm^3, tumor-bearing mice were either treated with control or anti-PD-L1 for 3 times every other day. Tumor volume was monitored in both tumor cell lines. **(A)** A1206C tumor growth curve. Control group (n=9) or aPD-L1 treatment group (n=9). (**B**) A1419C tumor growth curve. Control group (n=6) or aPD-L1 treatment group (n=6). **(C-F) OTX-008/anti-PD-L1 combo treatment.** 4-NQO-induced tumor cell lines, A1419C or A1206C (1×10^6) were injected s.c. at one flank of WT B6 recipients. When tumor size reached ~150mm^3, A1206C recipients were treated with control (n=10) or anti-PD-L1+OTX-008 (n=10, anti-PD-L1 on day 11, 13, 15 and OTX-008 on day 11, 13, 15, 17, 19, 21, 23). Tumor growth was monitored for 38 days. When tumor size reached ~150mm^3, A1419C recipients were treated with control (n=7) or anti-PD-L1+OTX-008 (n=8, anti-PD-L1 on day 14, 16, 18 and OTX-008 on day 14, 16, 18, 20, 22, 24, 26). Tumor growth was monitored for 32 days. **(C, E)** Overall tumor growth of control and treated recipients of A1206C **(C)** or A1419C **(E)**, respectively. Data were presented as mean ± SEM. Statistical significance was calculated with unpaired t test (*, P<0.05). **(D, F)** Individual tumor growth curves of A1206C **(D)** or A1419C **(F)** recipients, respectively, in different treatment groups.

Supplemental Figure 14A-F

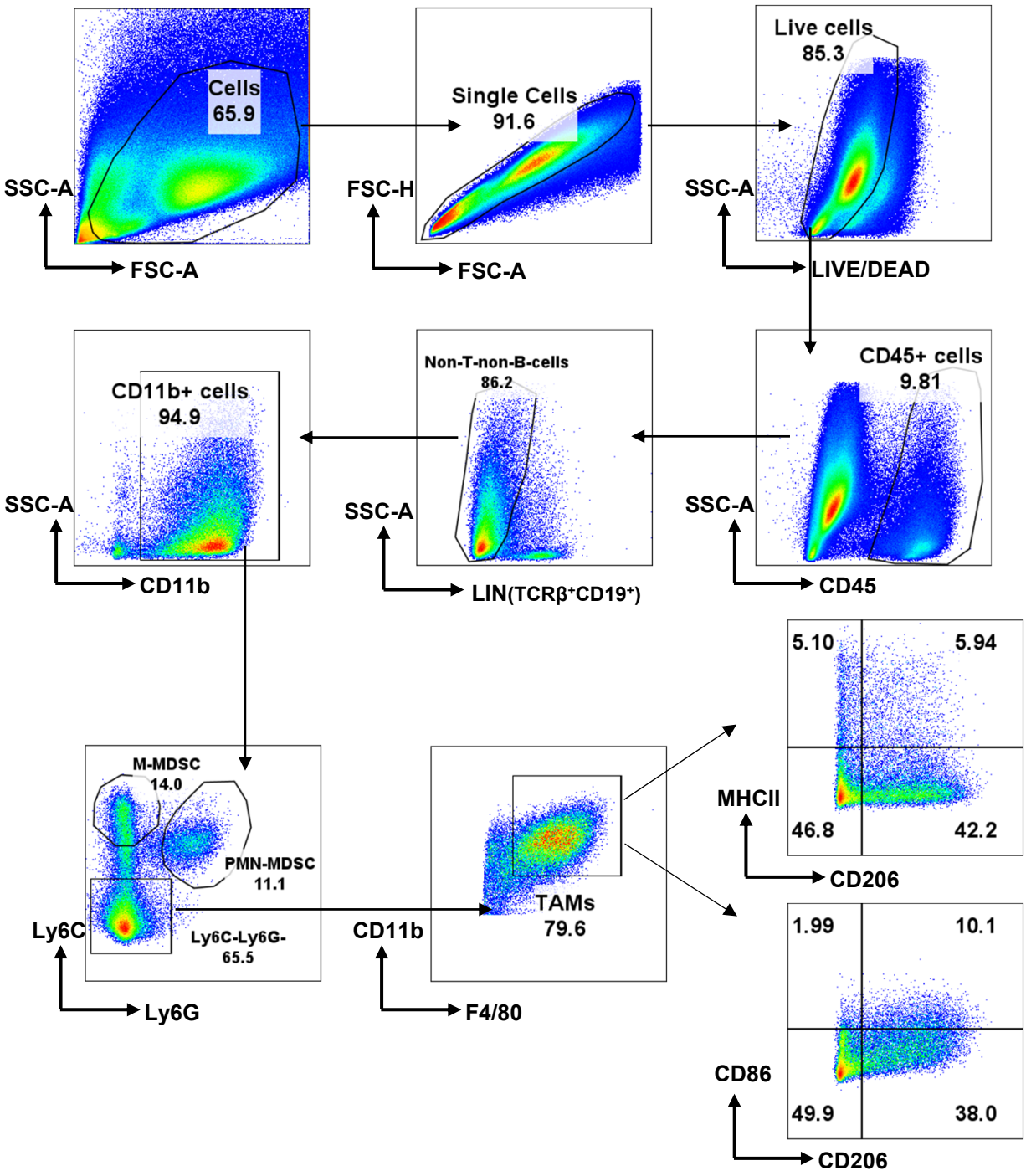

Supplemental Figure 15. Gating strategy for different subsets of myeloid cells. After gating on CD45$^+$ population, non-T/non-B population (TCRβ$^-$CD19$^-$) was gated. From the non-T/non-B population, CD11b$^+$ population was gated for myeloid cells. In the CD11b$^+$ population, we identified M-MDSC (Ly6C^{high}Ly6G$^-$) and PMN-MDSC (Ly6C^{low}Ly6G$^+$). For TAMs, we gated on Ly6C$^-$Ly6G$^-$ population, then gated on F4/80$^+$CD11b$^+$ population. For M2-TAMs, we gated on F4/80$^+$CD11b$^+$CD206$^+$CD86$^-$ population or F4/80$^+$CD11b$^+$CD206$^+$MHCII$^-$ population.

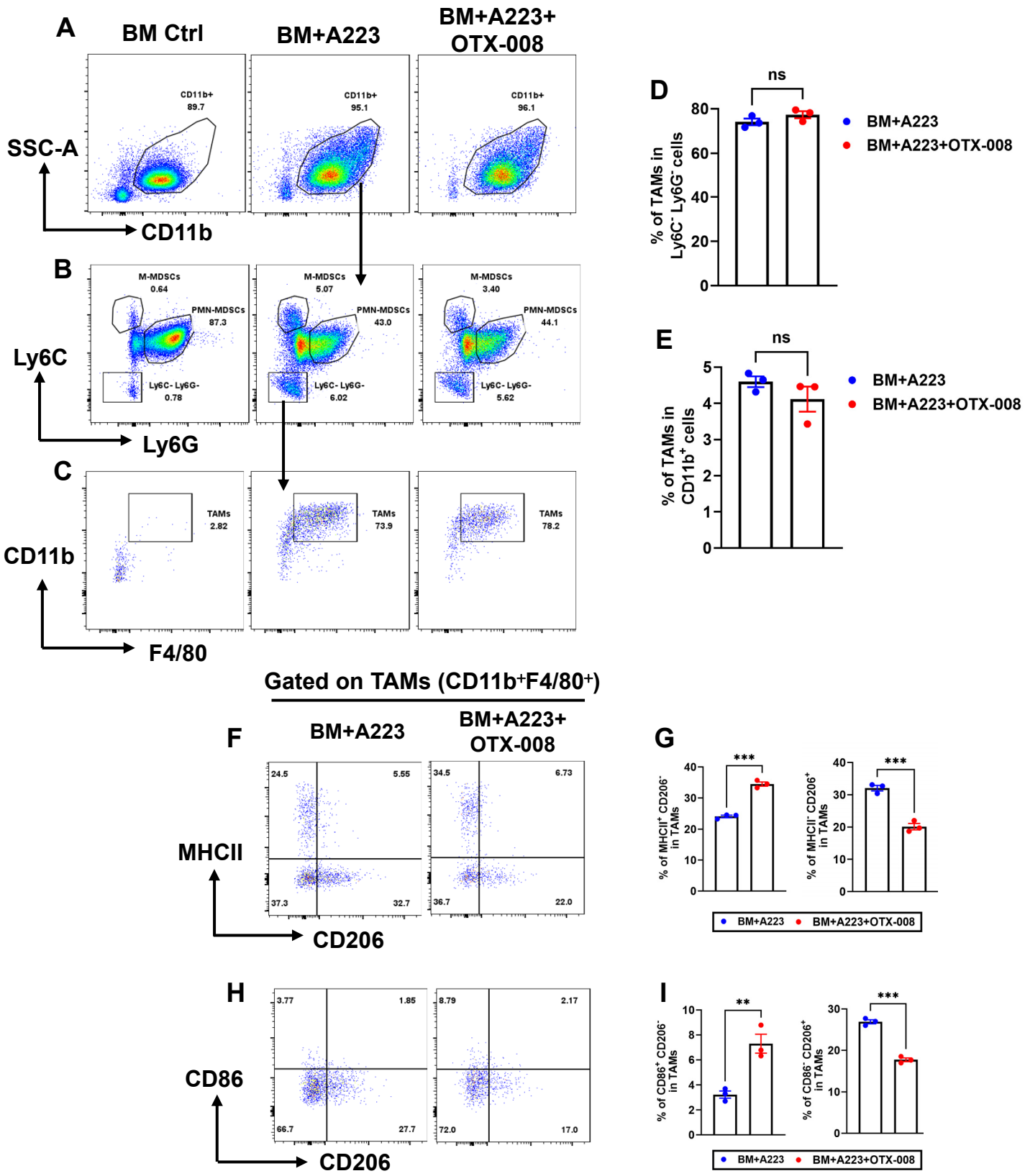

Supplemental Figure 16. OTX-008 modulated TAM polarization in a co-culture system of BM cells and A223 tumor cells. (A–C) Representative flow plots showing the gating strategy for TAMs: **(A)** $CD11b^+$ myeloid cells; **(B)** Separation of $CD11b^+$ cells into M-MDSCs ($Ly6C^+Ly6G^-$), PMN-MDSCs ($Ly6C^+Ly6G^+$) and double-negative cells ($Ly6C^-Ly6G^-$). **(C)** Identification of TAMs ($CD11b^+F4/80^+Ly6C^-Ly6G^-$). **(D-E)** Quantification of the percentage of TAMs in $CD11b^+Ly6C^-Ly6G^-$ population **(D)** or in total $CD11b^+$ population **(E)**. **(F, H)** Representative flow plots showing MHC-II vs. CD206 **(F)** or CD86 vs. CD206 **(H)** staining for TAM polarization into M1-like ($MHCII^+CD206^-$ or $CD86^+CD206^-$) or M2-like ($CD206^+MHCII^-$ or $CD206^+CD86^-$) phenotypes. **(G)** Quantification of the percentage of $MHCII^+CD206^-$ **(left)** and $MHCII^-CD206^+$ **(right)** TAMs. **(I)** Quantification of the percentage of $CD86^+CD206^-$ **(left)** and $CD86^-CD206^+$ **(right)** TAMs. Data represent mean ± SEM. Statistical significance was determined by unpaired t-test (**P < 0.01; ***P < 0.001; ns = not significant).

Supplemental Figure 16A-I

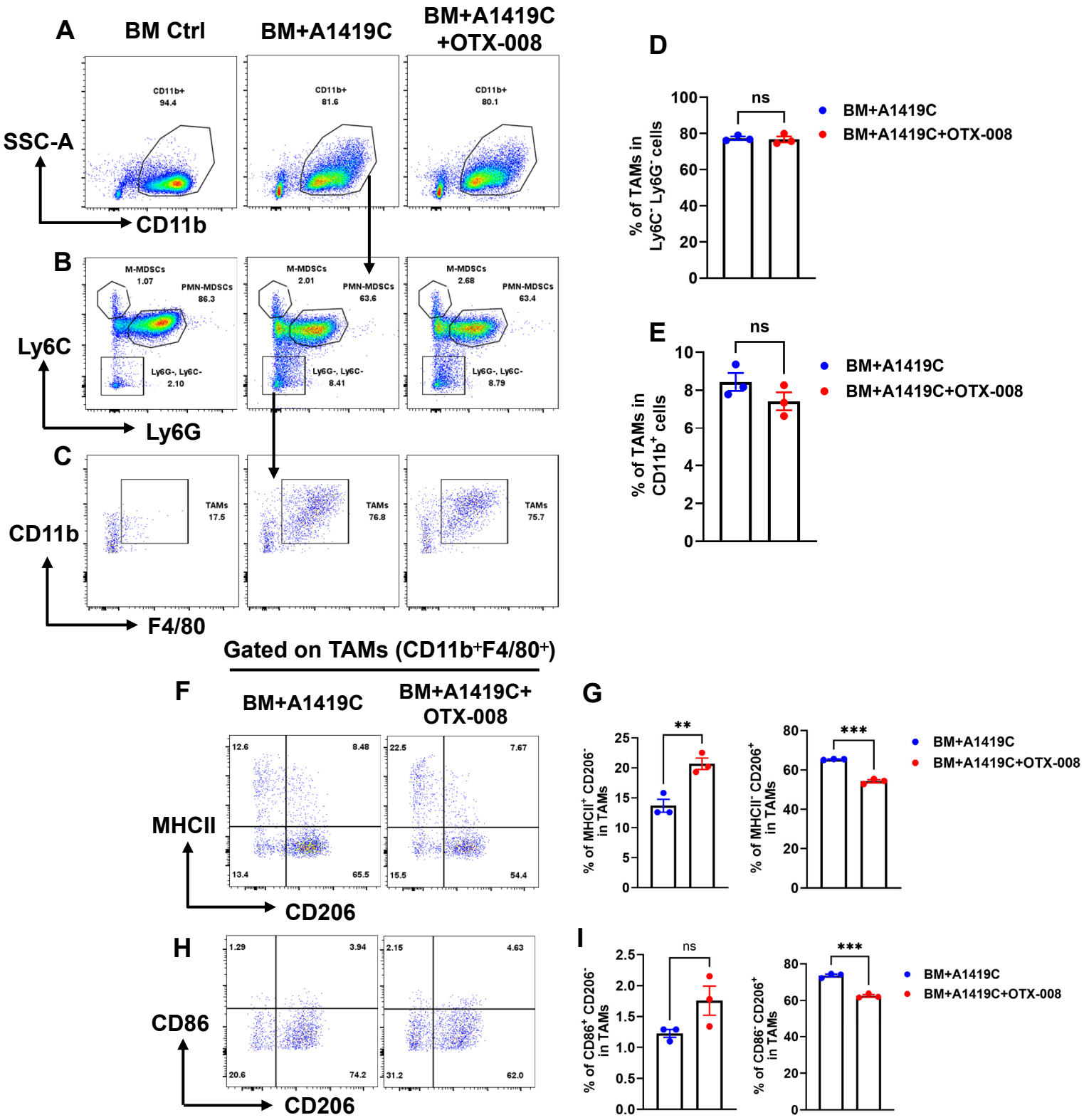

Supplemental Figure 17. OTX-008 modulated TAM polarization in a co-culture system of BM cells and A1419C tumor cells. (A–C) Representative flow plots showing the gating strategy for TAMs: **(A)** $CD11b^+$ myeloid cells; **(B)** Separation of $CD11b^+$ cells into M-MDSCs ($Ly6C^+Ly6G^-$), PMN-MDSCs ($Ly6C^+Ly6G^+$) and double-negative cells ($Ly6C^-Ly6G^-$). **(C)** Identification of TAMs ($CD11b^+F4/80^+Ly6C^-Ly6G^-$). **(D-E)** Quantification of the percentage of TAMs in $CD11b^+Ly6C^-Ly6G^-$ population **(D)** or in total $CD11b^+$ population **(E)**. **(F, H)** Representative flow plots showing MHC-II vs. CD206 **(F)** or CD86 vs. CD206 **(H)** staining for TAM polarization into M1-like ($MHCII^+CD206^-$ or $CD86^+CD206^-$) or M2-like ($CD206^+MHCII^-$ or $CD206^+CD86^-$) phenotypes. **(G)** Quantification of the percentage of $MHCII^+CD206^-$ **(left)** and $MHCII^-CD206^+$ **(right)** TAMs. **(I)** Quantification of the percentage of $CD86^+CD206^-$ **(left)** and $CD86^-CD206^+$ **(right)** TAMs. Data represent mean ± SEM. Statistical significance was determined by unpaired t-test (**P < 0.01; ***P < 0.001; ns = not significant).

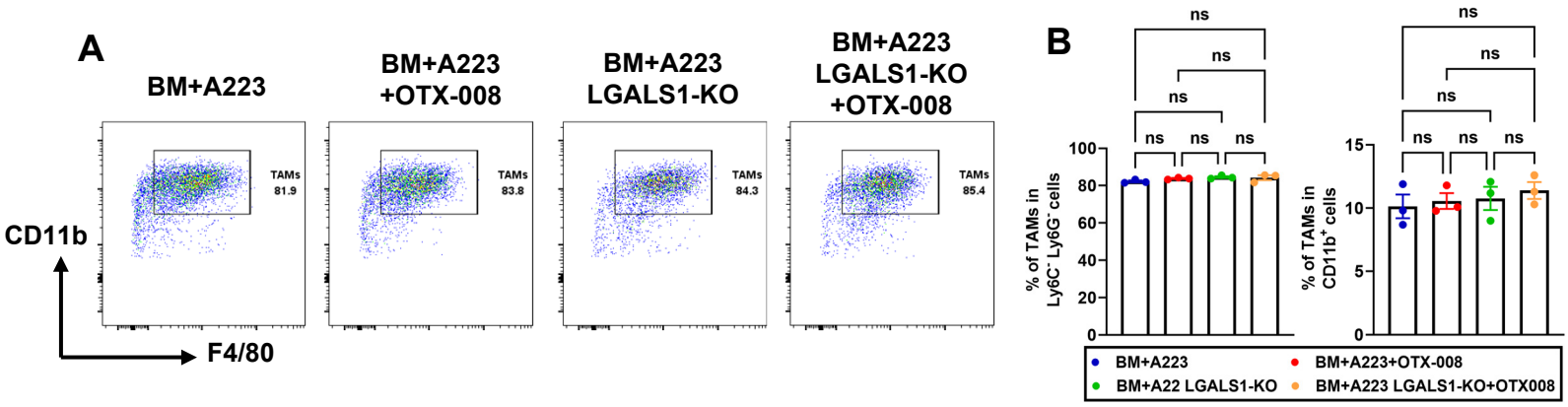

Supplemental Figure 18. Effects of OTX-008 treatment on TAMs. OTX-008 does not affect the percentage of TAMs in the co-culture of BM cells with wild-type (WT) or LGALS1-knockout (KO) A223 tumors. **(A)** Representative flow cytometry plots for TAM ($CD11b^+F4/80^+$). **(B)** Quantification of the percentage of TAMs in $CD11b^+Ly6C^-Ly6G^-$ population **(left)** or in total $CD11b^+$ population **(right)**. Data were presented as mean ± SEM. Statistical significance was calculated with two-way ANOVA followed by Tukey's multiple comparisons test (ns, not significant).

Supplemental Figure 18A, B

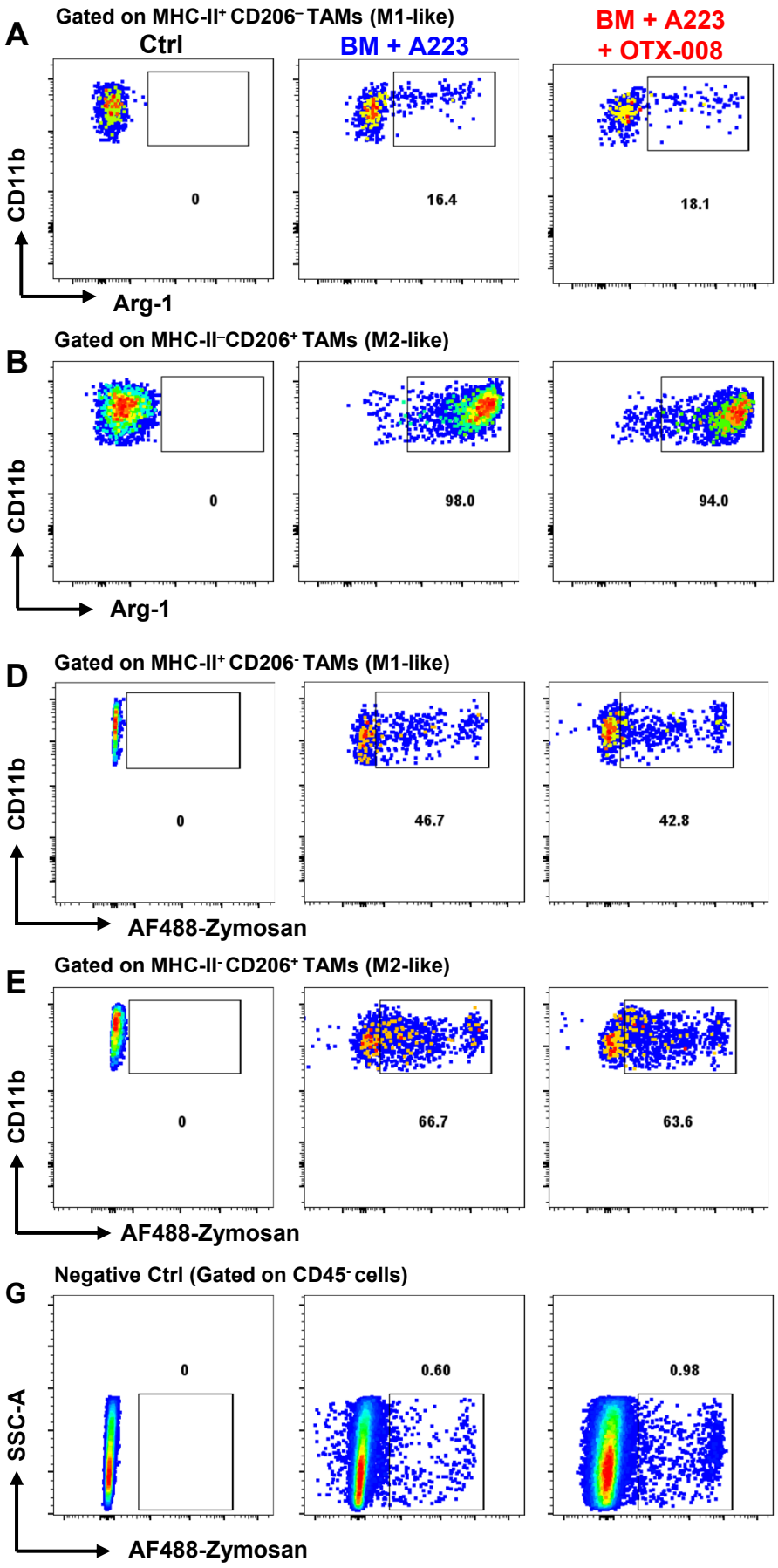

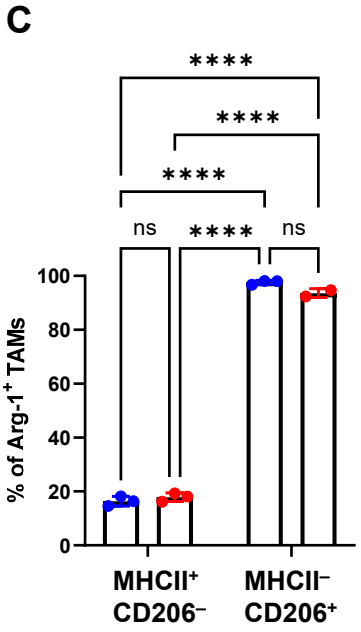

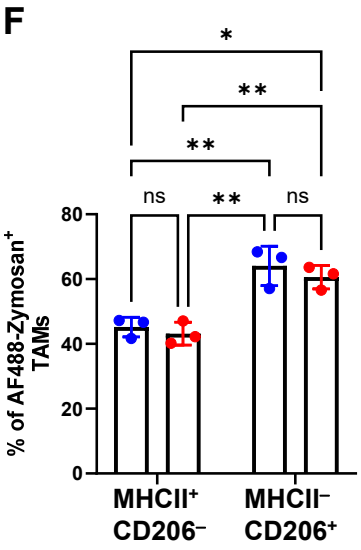

Supplemental Figure 19. Functional validation of TAM subsets. (A,B) Representative flow cytometry plots showing intracellular Arginase-1 (Arg-1) expression in **(A)** M1-like (MHCII$^+$ CD206$^-$) and **(B)** M2-like (CD206$^+$ MHCII$^-$) TAMs (CD11b$^+$F4/80$^+$Ly6C$^-$Ly6G$^-$). **(C)** Quantification of the percentage of Arg-1 expressing cells in M1-like and M2-like TAMs. **(D,E)** Representative flow plots showing the phagocytosis of Alexa Fluor 488-conjugated Zymosan particles by **(D)** M1-like and **(E)** M2-like TAMs, with **(F)** corresponding quantification of phagocytic activity. **(G)** Representative flow plots of Zymosan uptake by A223 tumor cells, serving as an assay negative control. Data were presented as mean ± SEM. Statistical significance was determined via two-way ANOVA followed by Tukey's multiple comparisons test (ns, not significant; **P*<0.05; ***P*<0.01; ****P*<0.001; *****P*<0.0001).

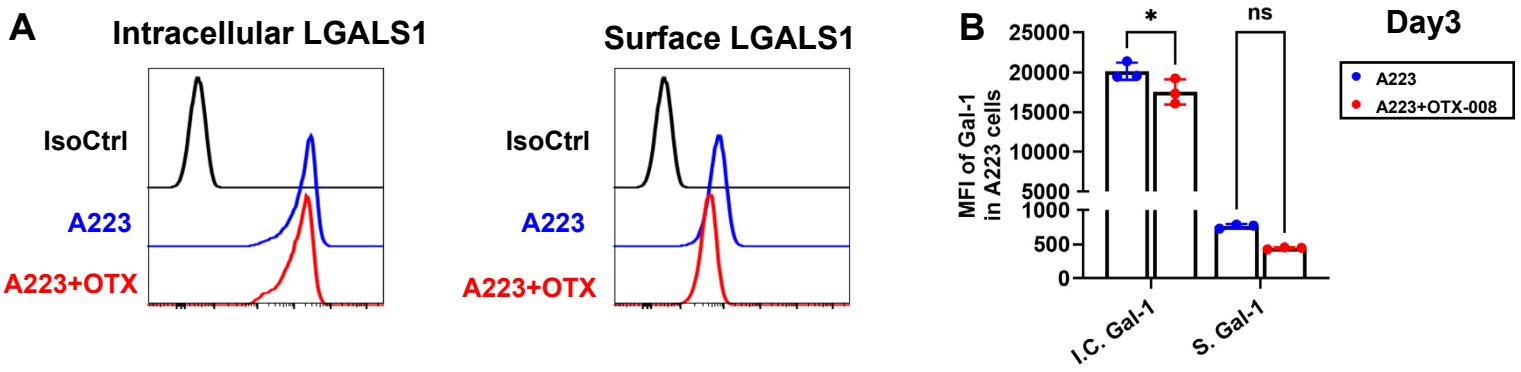

Supplemental Figure 20. Effects of OTX-008 on LGALS1 expression in A223 tumor cells *in vitro*. **(A)** Representative flow plots of intracellular or surface LGALS1 expression in A223 tumor cells on day 3 of OTX-008 treatment *in vitro*. **(B)** Quantification of MFI for intracellular or surface expression of LGALS1. Data were presented as mean ± SEM. Statistical significance was calculated with two-way ANOVA followed by Tukey's multiple comparisons test (ns, not significant; *, P<0.05).

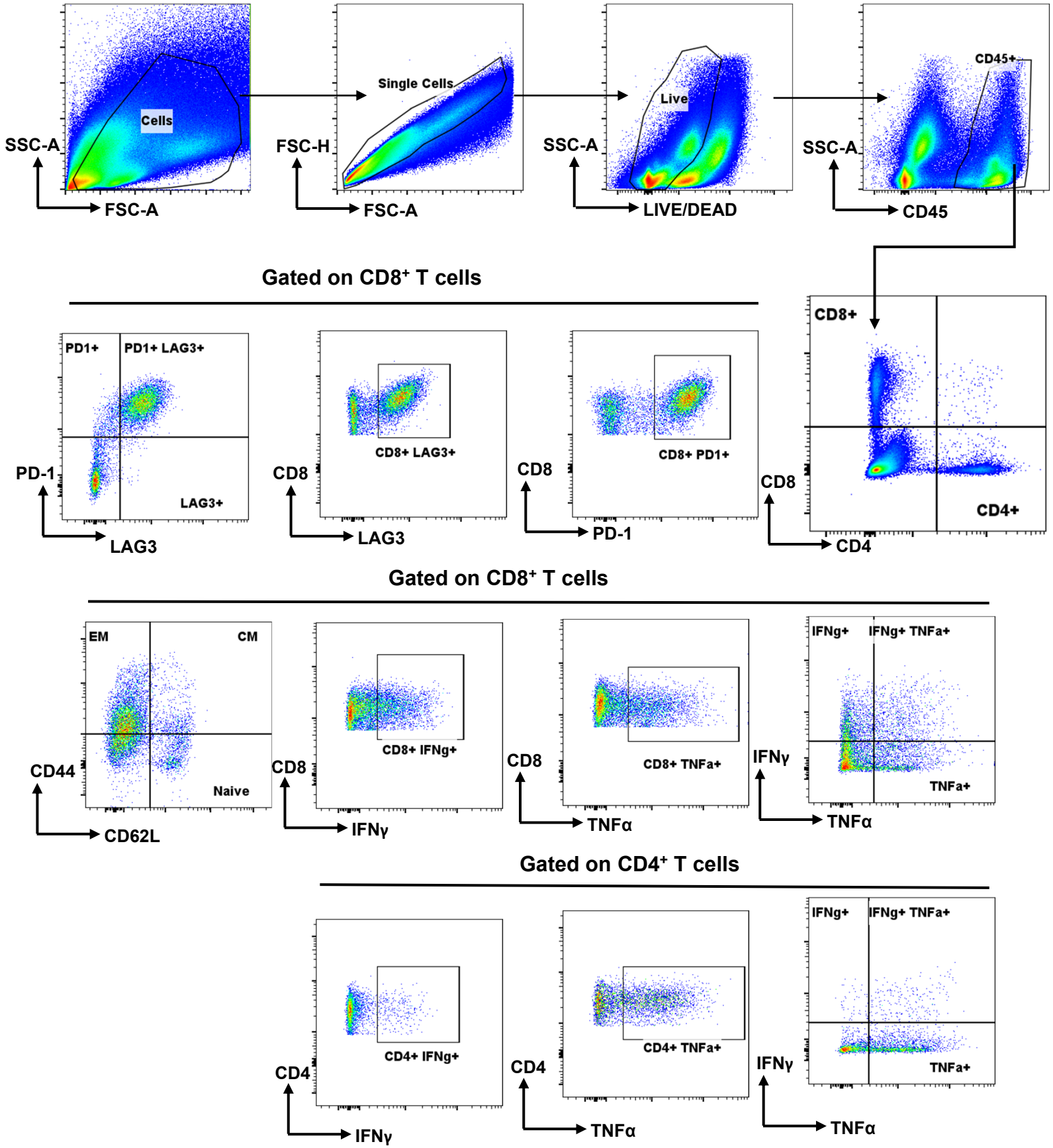

Supplemental Figure 21. Gating strategy for different subsets of T cells. After gating on the CD45$^+$ population, CD8$^+$ and CD4$^+$ T cells were identified. Expression of immune checkpoint molecules (PD-1 and LAG-3) was assessed on CD8$^+$ T cells. Naïve, effector memory, and central memory CD8$^+$ T cell subsets were defined based on CD44 and CD62L expression. Cytokine production by CD4$^+$ and CD8$^+$ T cells was evaluated by intracellular staining for IFN-γ and TNF-α.

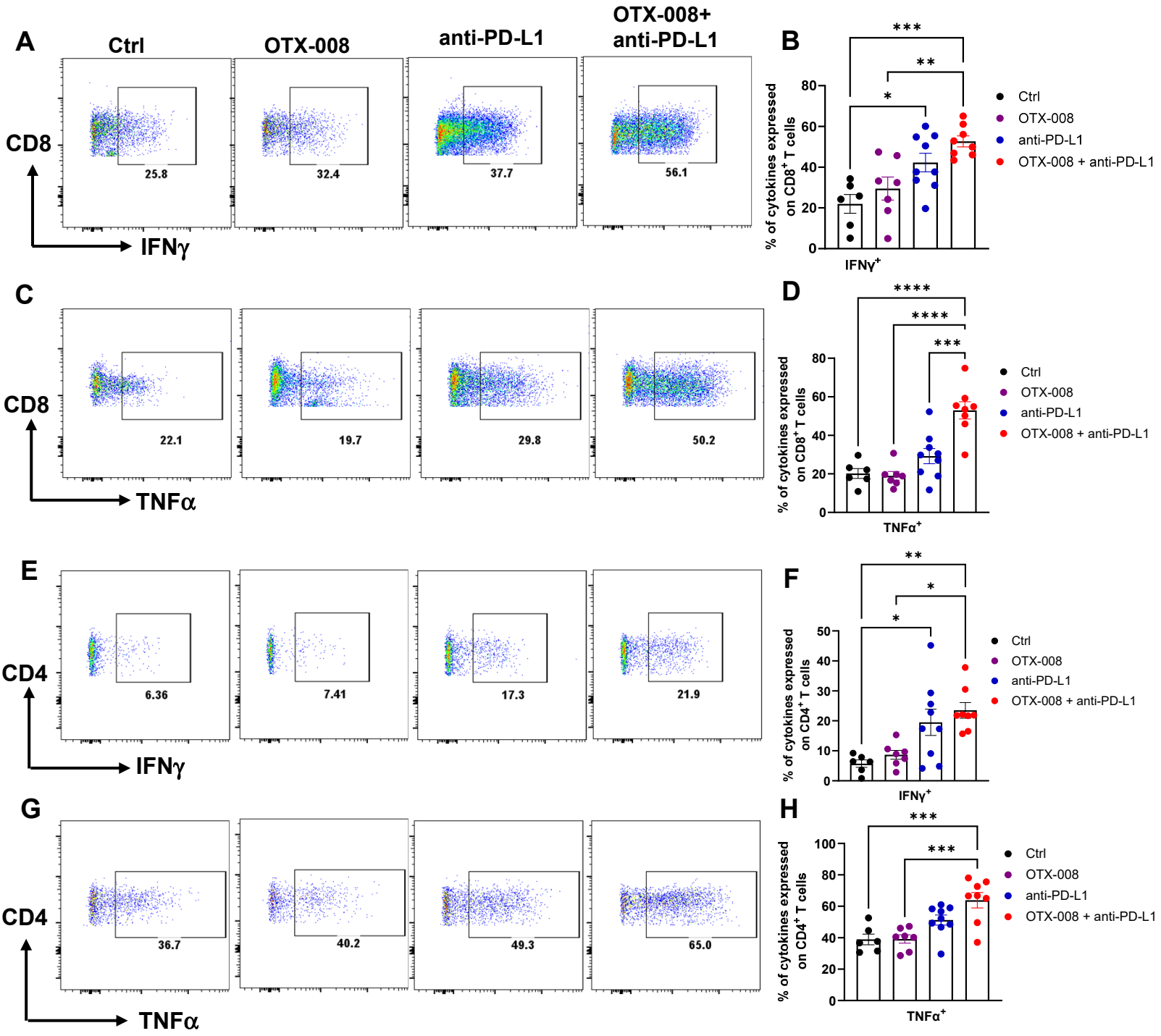

Supplemental Figure 22: Combination treatment of OTX-008 and anti-PDL1 activates CD4 and CD8 TILs *in vivo*. A223 tumors were injected into WT B6 mice and tumor-bearing mice were treated as described in Figure 3. Tumors were harvested, and cells were stained and analyzed by flow cytometry on day 26 after tumor injection. Representative flow plots **(A, C, E, G)** and quantification of the percentages **(B, D, F, H)** of activated CD8 and CD4 TILs producing IFNγ or TNFα cytokines in different treatment groups. Control (Ctrl, n=6), OTX-008 (n=7), anti-PD-L1 (n=9) and combination (OTX-008+anti-PD-L1, n=8). Data were presented as mean ± SEM. Statistical significance was calculated with one-way ANOVA followed by Tukey's multiple comparisons test (*, *P*<0.05; **, *P*<0.01; ***, *P*<0.001; ****, *P*<0.0001).

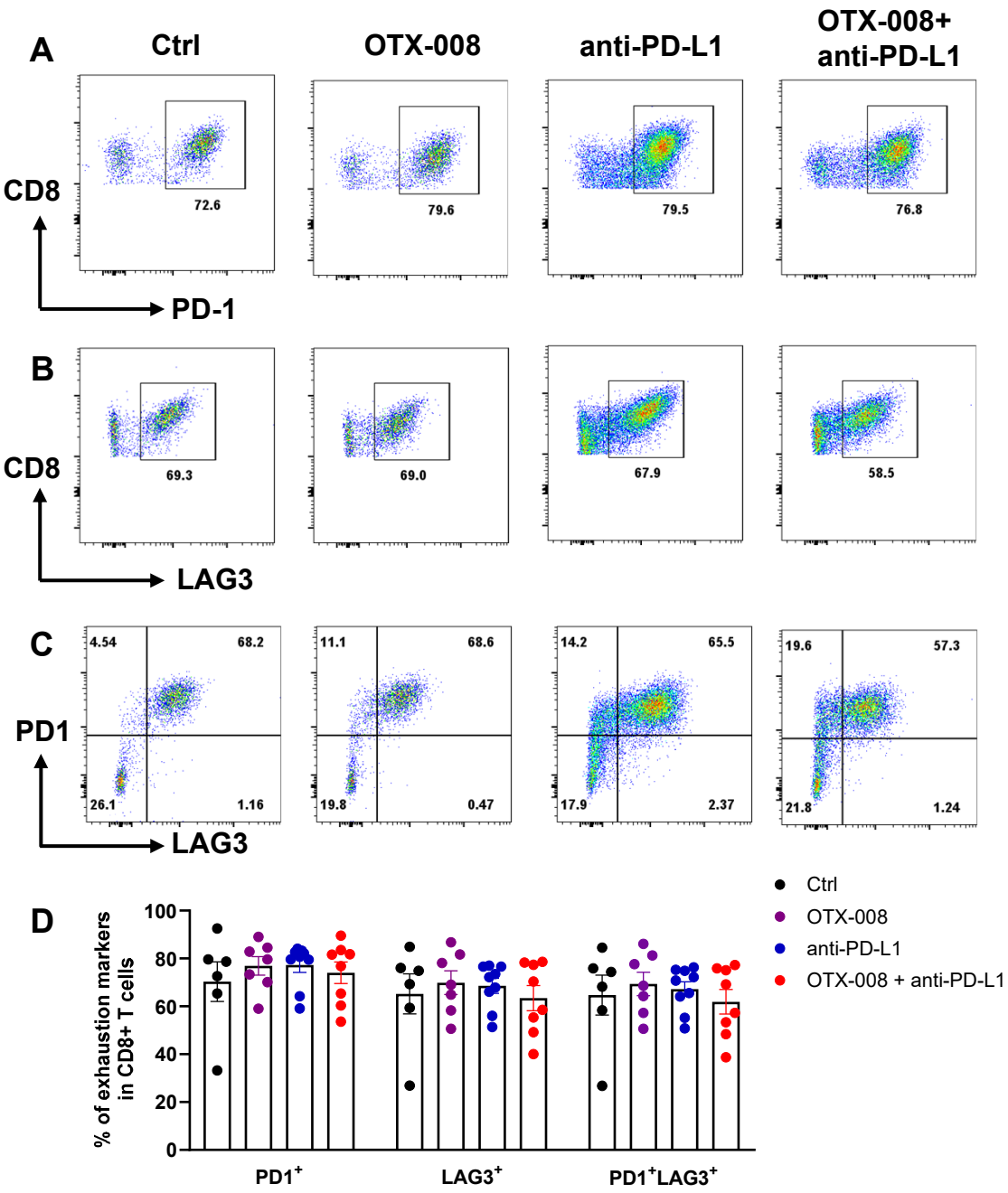

Supplemental Figure 23. Effect of combination treatment on the expression of checkpoint molecules on CD8 TILs. A223 tumors were injected into WT B6 mice and tumor-bearing mice were treated as described in Figure 3. Tumors were harvested, and cells were stained and analyzed by flow cytometry on day 26 after tumor injection. **(A-D)** PD-1 and LAG-3 expression in CD8 TILs. Representative flow plots showing the expression of PD-1 **(A)**, LAG-3 **(B)**, and co-expression of PD-1 and LAG-3 **(C)** on CD8 TILs from control (Ctrl, n=6), OTX-008 (n=7), anti-PD-L1 (n=9) and combination (OTX-008+anti-PD-L1, n=8) treatment groups. **(D)** Quantification of the percentage of CD8 TILs expressing checkpoint molecules in different groups. Data were presented as mean ± SEM. Statistical significance was calculated with one-way ANOVA followed by Tukey's multiple comparisons test (*, $P<0.05$; **, $P<0.01$).

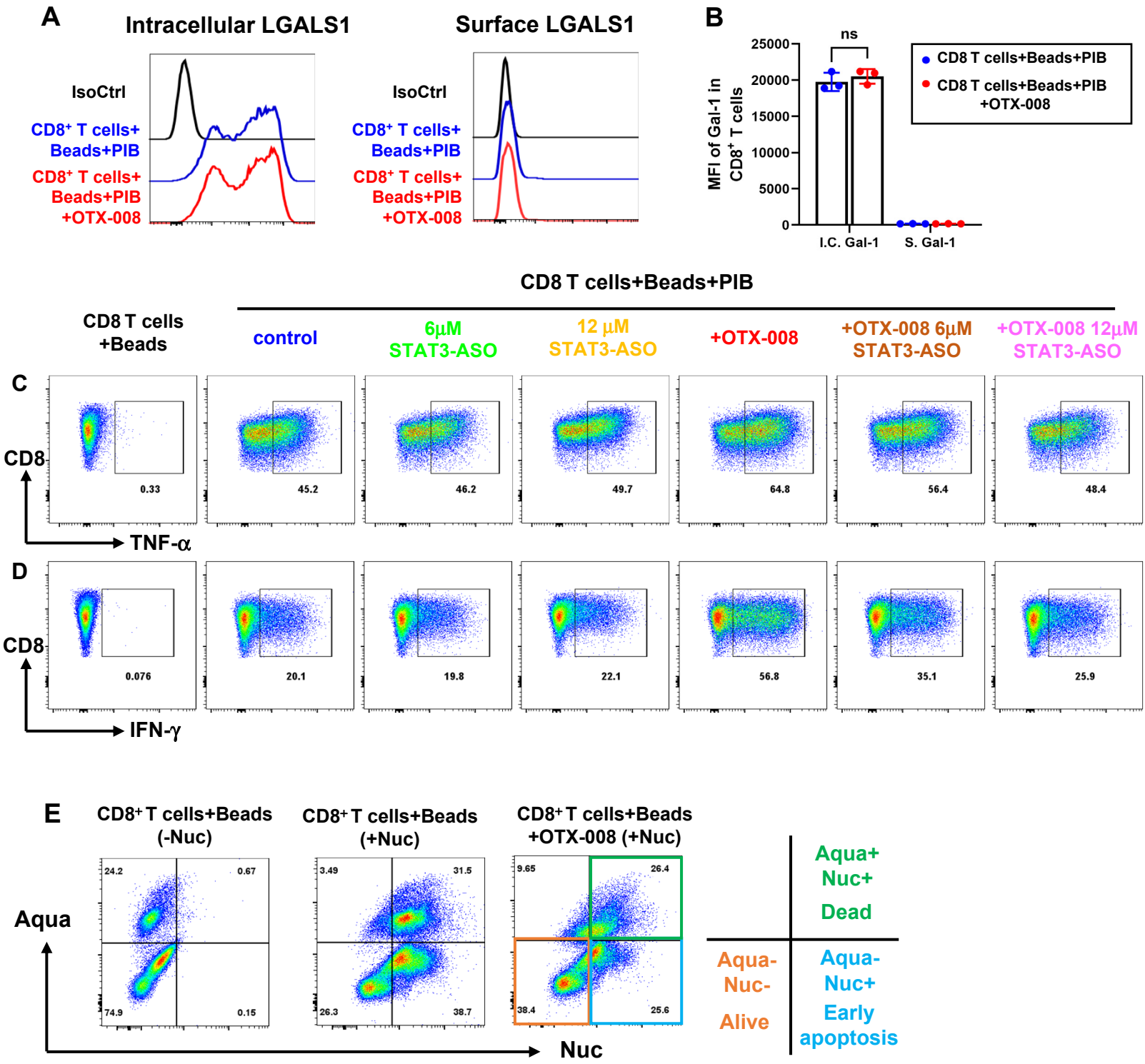

Supplemental Figure 24. Effects of OTX-008 treatment on CD8 T cells. (A, B) OTX-008 does not affect the expression of LGALS1 in anti-CD3/anti-CD28-beads activated CD8⁺ T cells. **(A)** Representative flow plots showing intracellular or surface LGALS1 expression in activated CD8⁺ T cells with or without OTX-008. **(B)** Quantification of MFI for surface and intracellular LGALS1 expression in activated CD8⁺ T cells with or without OTX-008. **(C, D)** OTX-008 enhanced CD8 T cell effector function in a STAT3-dependent manner. Representative flow plots showing the expression of cytokine TNF-α **(C)** or IFN-γ **(D)** in CD8⁺ T cells stimulated with anti-CD3/CD28 beads and treated with either STAT3-specific ASO (6 μM or 12 μM), OTX-008 or their combination. For cytokine staining, cells were stimulated with a cocktail of PMA, Ionomycin and BFA (PIB) for 4hrs before flow analysis. **(E)** Representative flow plots showing that OTX-008 treatment reduced the level of cell death in activated CD8⁺ T cells.

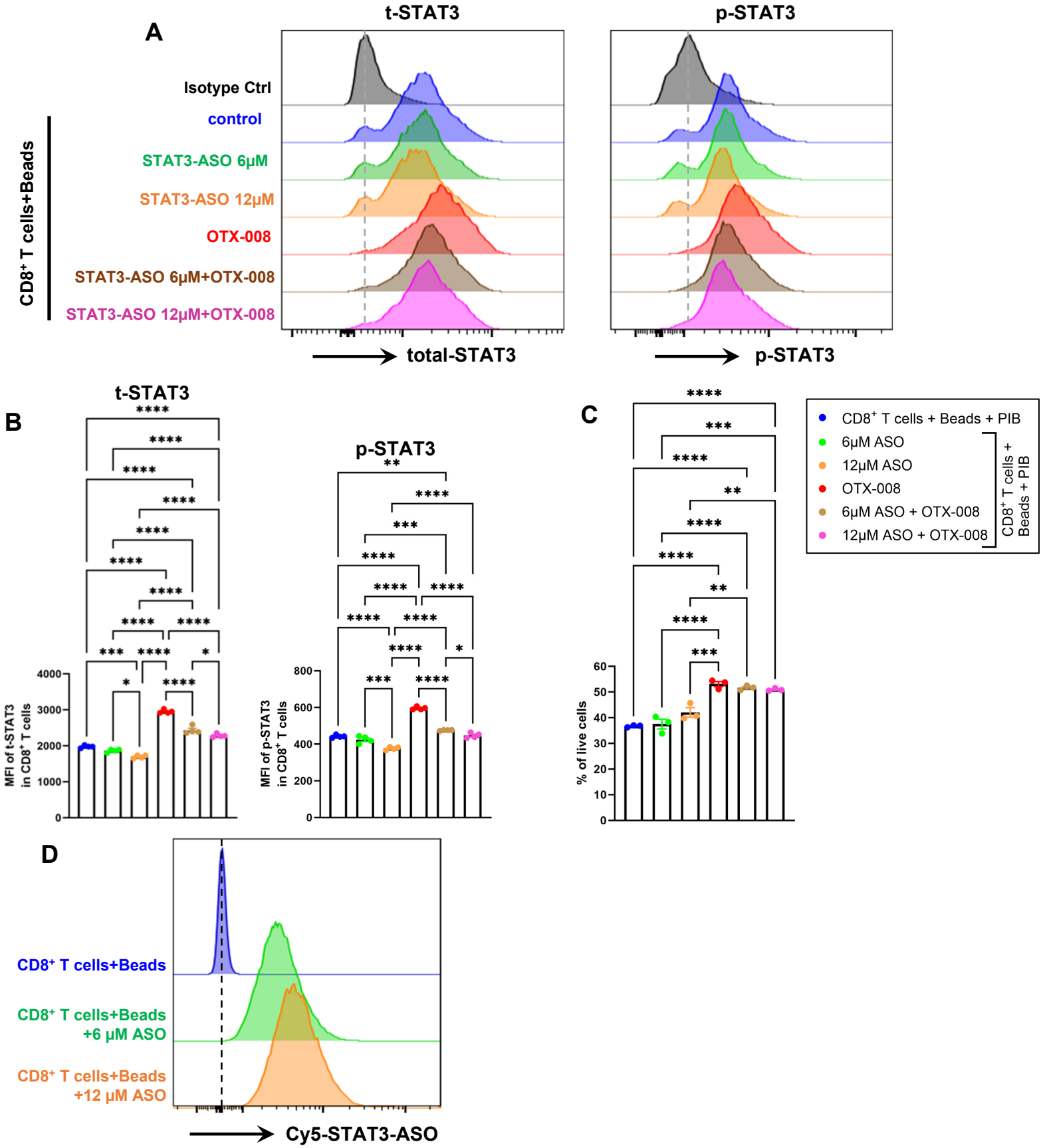

Supplemental Figure 25. STAT-3-ASOs abrogated OTX-008-induced upregulation of STAT3 in activated CD8 T cells. (A) Representative flow histograms showing the expression level of total STAT3 (t-STAT3) and phosphorylated STAT3 (p-STAT3) measured by mean fluorescence intensity (MFI) in CD8 T cells stimulated with anti-CD3/CD28 beads and treated with STAT3-ASOs, OTX-008 or their combination. **(B)** Quantification of MFI for t-STAT3 and p-STAT3 in CD8 T cells from the experiment shown in **(A)**. **(C)** Quantification of CD8 T cell viability, based on Aqua live/dead staining, following treatment with STAT3-ASOs, OTX-008 or their combination. **(D)** Representative flow histograms demonstrating uptake of Cy5-labeled STAT3-ASOs by CD8 T cells. Data represent mean ± SEM. Statistical significance was calculated using two-way ANOVA followed by Tukey's test (*$P < 0.05$, **$P < 0.01$, ***$P < 0.001$, ****$P < 0.0001$).

Supplemental Figure 25A-D

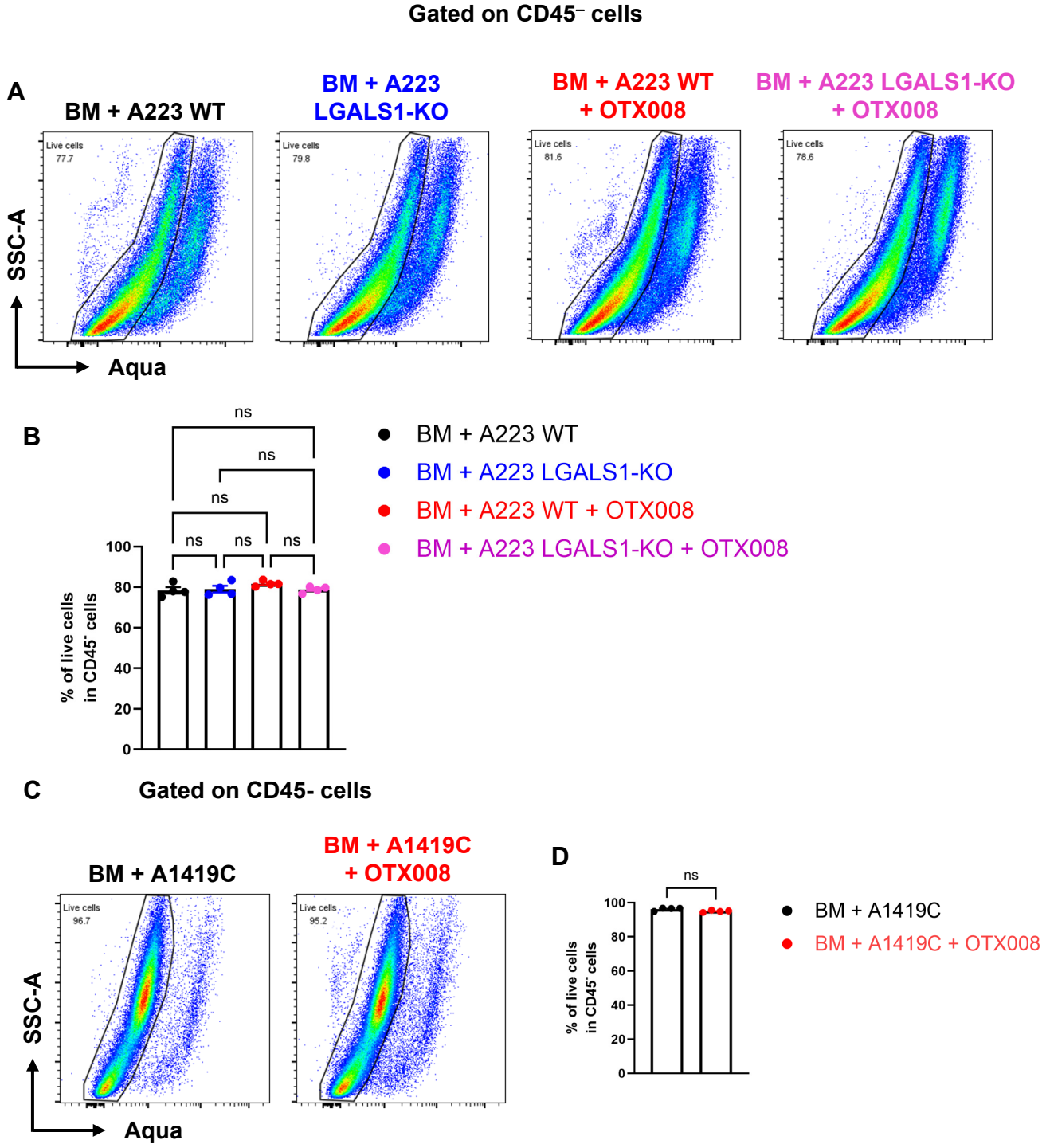

Supplemental Figure 26. OTX-008 treatment had no effects on viability of tumor cells in co-culture assay. Tumor cells were cultured with BM cells for 4 days in the presence or absence of OTX-008 (10μM) as described in Method. **(A)** Representative flow cytometry plots showing Aqua live/dead staining of WT or LGALS1-KO A223 tumor cells ($CD45^-$) with or without OTX-008 treatment. **(B)** Quantification of live A223 WT or LGALS1-KO tumor cells with or without OTX-008 treatment. **(C)** Representative flow cytometry plots showing Aqua live/dead staining of A1419C tumor cells ($CD45^-$) with or without OTX-008. **(D)** Quantification of live A1419C tumor cells. Data represent mean ± SEM. Statistical significance was calculated with two-way ANOVA followed by Tukey's test in **(B)** or with an unpaired t-test in **(D)** (ns = not significant).

Targeting molecules like LGALS1 affecting tumor cells, myeloid and CD8 T cells simultaneously to promote anti-tumor immunity

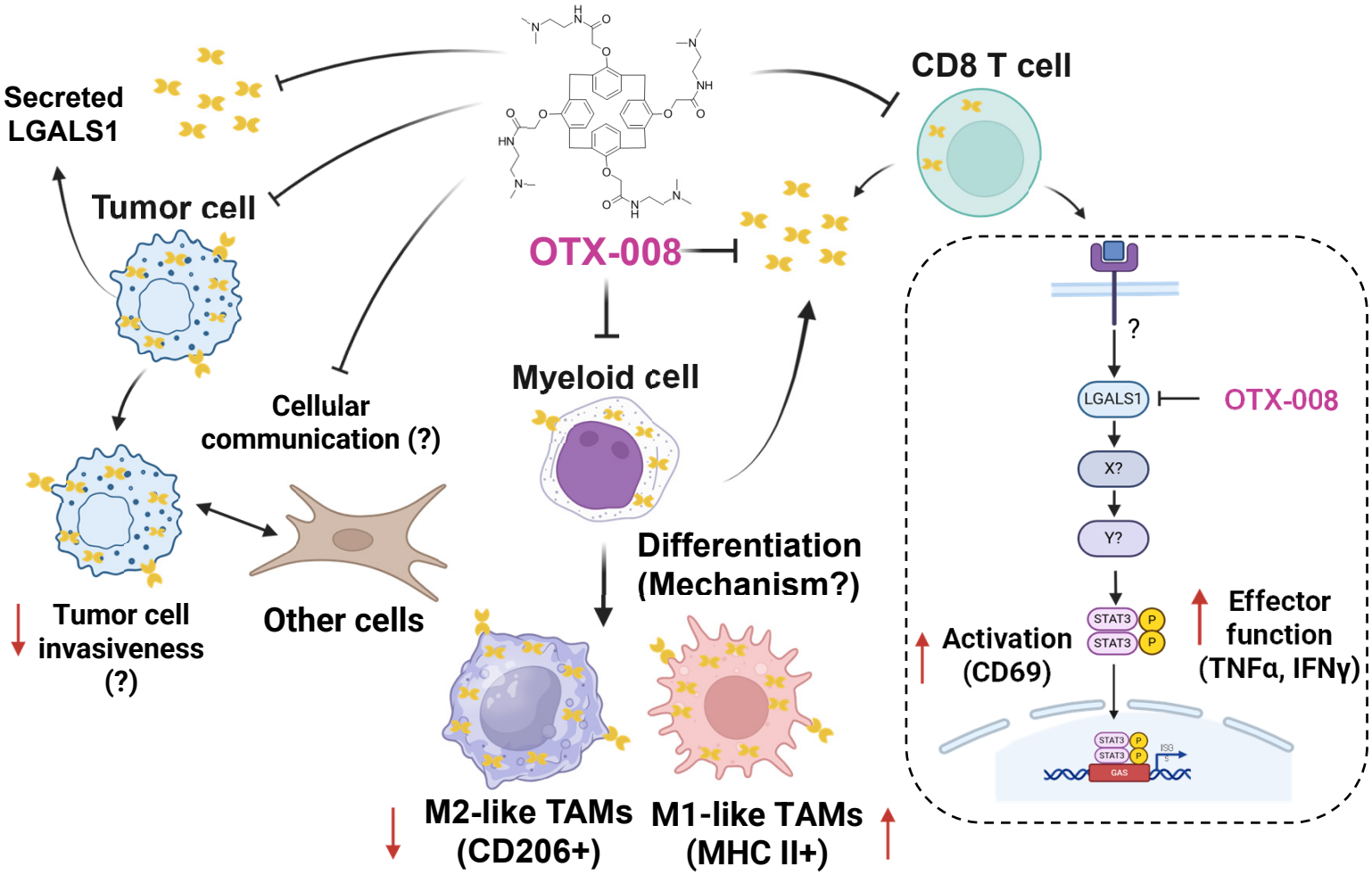

Supplemental Figure 27. Proposed mechanisms of LGALS1 blockade to enhance anti-tumor immunity. OTX-008 can block LGALS1 expressed in tumor, myeloid and CD8 T cells or secreted LGALS1 outside of cells. Several mechanistic questions remain to be addressed including the role of LGALS1 in CD8 T cell activation and survival, in myeloid cell differentiation and in tumor cells' phenotypic changes.